

April 2011

Photoelectrocatalytic Study of Gold-Modified Bismuth Vanadate for the Degradation of 4-Chlorophenol

Andrew Paul Black
Worcester Polytechnic Institute

Follow this and additional works at: <https://digitalcommons.wpi.edu/mqp-all>

Repository Citation

Black, A. P. (2011). *Photoelectrocatalytic Study of Gold-Modified Bismuth Vanadate for the Degradation of 4-Chlorophenol*. Retrieved from <https://digitalcommons.wpi.edu/mqp-all/3356>

This Unrestricted is brought to you for free and open access by the Major Qualifying Projects at Digital WPI. It has been accepted for inclusion in Major Qualifying Projects (All Years) by an authorized administrator of Digital WPI. For more information, please contact digitalwpi@wpi.edu.

Photoelectrocatalytic Study of Gold-Modified BiVO_4 for the Degradation of 4-Chlorophenol



A WPI Major Qualifying Project

By Andrew Black

Sponsored by



上海交通大學

Shanghai Jiao Tong University

School of Environmental Science and Engineering



Photoelectrocatalytic Study of Gold-Modified BiVO₄ for the Degradation of 4-Chlorophenol

A Major Qualifying Project Report
submitted to the faculty of

Worcester Polytechnic Institute

in partial fulfillment of the requirements for the
Degree of Bachelor of Science

By

Andrew Black

On

April 27, 2011

Dr. Hong Susan Zhou, Assistant Professor
Worcester Polytechnic Institute
Department of Chemical Engineering
Shanghai Major Qualifying Project Center

In Cooperation With

Dr. Mingce Long, Assistant Professor
Shanghai Jiao Tong University
School of Environmental Science and Engineering

Project Number HSZ-CH01

Abstract

This project, prepared in collaboration with Shanghai Jiao Tong University, details a study on the modification of monoclinic BiVO_4 photocatalyst with gold nanoparticles for the degradation of 4-chlorophenol. It adapts methodologies in the literature for the synthesis of thin film semiconductor photocatalyst electrodes and photoelectrochemical characterization techniques, including linear sweep and cyclic voltammetry and chopped irradiation chronoamperometry, to compare BiVO_4 modified with 0.5, 0.75, 1, 2, and 4 wt% gold to its unmodified form. Additional parameters explored were the material of the counter electrode, the electrical potential bias, the spectra of illumination, and the addition of hydrogen peroxide. Analysis of data suggested that 2 wt% Au/BiVO_4 was the most suitable thin film electrode for the degradation of 4-chlorophenol in a $\text{H}_2\text{O}_2\text{-Na}_2\text{SO}_4$ electrolyte. Several recommendations for improving the quality of the research are then discussed.

Acknowledgments

I would like to thank the School of Environmental Science and Engineering at Shanghai Jiao Tong University for providing me with the fortuity to participate in this project and great cultural exchange. Specifically, my thanks extend to Professor Mingce Long, my lab advisor, whose support and aid were invaluable to the completion of this project. The generosity to graciously provide the workspace, materials, and equipment required for this project is greatly appreciated. I would like to thank Professor Jiahui Shao at SJTU and Professors David DiBiasio and Susan Zhou at WPI for organizing this experience. Additional thanks go to Professor Zhou for supervising the writing of this report.

Special thanks go to the members of the lab and other Chinese students befriended while abroad for introducing me to weird yet delicious food, for helping me acclimate to the culture of China, and for enabling me to truly reap the benefits of an experience abroad. Their persistent willingness to help and hospitality deserves this acknowledgement. Many thanks go to my dorm-mates and WPI classmates for enjoying with me the amazing opportunities that China offers and ensuring that I did not go crazy.

Table of Contents

Abstract	i
Acknowledgments	ii
Table of Contents	iii
List of Figures	iv
List of Tables	iv
Chapter 1: Introduction	1
Chapter 2: Background	3
2.1 Motivation for Semiconductor Photocatalysis	3
2.2 Basics of Semiconductor Photocatalysis	4
2.3 Photocatalysts with Metal Nanoparticle Modification	7
Chapter 3: Methodology	10
3.1 Synthesis of Catalyst Paste	11
3.2 Preparation of FTO Glass Electrode	12
3.3 Assembly of Electrochemical Cell	13
3.4 Characterization	15
3.4.1 Linear Sweep Voltammetry	15
3.4.2 Chronoamperometry	15
3.4.3 Degradation of 4-Chlorophenol	16
3.4.4 SEM	17
Chapter 4: Results and Discussion	18
4.1 Linear Sweep Voltammetry	18
4.2 Chronoamperometry	21
4.3 Degradation of 4-Chlorophenol	24
4.4 SEM Images	27
4.5 Errors and Lab Practices	28
4.6 Recommendations for Future Work	30
Chapter 5: Conclusions	34
References	35
Appendix	38
Furnace Program for Electrode Calcination	38
SEM Images	38

List of Figures

Figure 1: Basic schematic of a photoelectrochemical cell with an n-type semiconductor	5
Figure 2: Schematic of major processes following $e^- h^+$ photogeneration.....	6
Figure 3: Charge separation in a TiO_2 or BiVO_4 electrode	9
Figure 4: Schematic of the overall methodology	11
Figure 5: Temperature-time profile of the electrode calcination program	13
Figure 6: Bismuth vanadate in a vial and doctor bladed on three FTO glass electrodes and the same electrodes after calcination	13
Figure 7: Pictures of the electrochemical cell.....	14
Figure 8: The experimental setup for 4-chlorophenol degradation.	16
Figure 9: The working electrodes after calcination coated with a thin film of Au/BiVO_4	18
Figure 10: Linear sweep voltammetry	20
Figure 11: CVs performed with BiVO_4 electrode before photocurrent measurements	21
Figure 12: Chronoamperometric photocurrent measurements at constant potentials.....	23
Figure 13: Chronoamperometric photocurrent measurements with different filters	24
Figure 14: Absorbance of samples from 4-chlorophenol degradation with 2 wt% Au/BiVO_4	25
Figure 15: Absorbance of samples from 4-chlorophenol degradation with 2 wt% Au/BiVO_4 and 5 mM H_2O_2 added.....	26
Figure 16: Absorbance of samples from 4-chlorophenol degradation with 2 wt% Au/BiVO_4 and 10 mM H_2O_2	27
Figure 17: SEM images BiVO_4 , 1 wt% BiVO_4 , and 2 wt% Au/BiVO_4	28

List of Tables

Table 1: Processes and characteristic times in TiO_2 photomineralization of organics	7
Table 2: Magnifications of SEM images for 0, 0.5, 1, and 2 wt% Au/BiVO_4	17

Chapter 1: Introduction

Contamination of water by organic pollutants significantly impacts developed and rapidly developing regions in the world. Without proper treatment, they seep into groundwater aquifers, rivers, and reservoirs used as water sources. The slow pace of hazardous waste remediation means that the presence of toxic chemical substances from waste effluents and previously contaminated sites is a major concern.¹

Mineralization (oxidation of organic compounds to carbon dioxide, water, and other inorganic components) by photoelectrochemical methods has been identified as an effective waste degradation technique with applications in environmental control technology by semiconductor photocatalysis with TiO_2 and BiVO_4 .¹ A supreme challenge for photocatalysis century is the development of new catalysts that more efficiently utilize sunlight, a vastly abundant and green energy source, to drive chemical reactions of interest to society. This research has led to great new understandings of heterogeneous photocatalysis by metal oxide systems in environments with multiple phases.^{2,3}

Heterogeneous titanium dioxide photocatalysts are well-studied in the removal of organic pollutants from environments and are known to be highly oxidative, inexpensive, non-toxic, and chemically stable; however, these advantageous properties are offset by the fact that TiO_2 is active only under UV light irradiation. Because ambient light is typically provided by the sun or conventional fluorescent lamps, it is desirable to develop visible-light driven photocatalysts that demonstrate degradation activity on the order of titanium dioxide.⁴⁻⁷ Bismuth vanadate is one such candidate that has shown promising photooxidation capabilities under visible light irradiation. Its activity is typically improved by the loading of transition metals such as silver or gold.^{6,8-10} In particular, gold nanoparticles are known to strongly absorb visible light due to a surface plasmon resonance effect.²

Nanocrystalline semiconductor thin films exhibit a highly microporous structure with similar properties to semiconductor particle suspensions. The use of an immobilized thin film eliminates the need to add semiconductor particles to a reaction mixture and then perform a separation step. Developments in designing porous nanocrystalline thin films make it possible to achieve charge separation in a semiconductor system with an electrochemical bias.^{4,6,11-13}

4-Chlorophenol was chosen as a model organic compound. Chlorophenol compounds are used in disinfectant agents and pesticides and are intermediates in the polychlorination of phenol. Exposure is most common after water is disinfected with chlorine, wood is bleached, and pesticides released to the environment go into water. High levels of chlorophenols cause liver and immune system effects and may lower birth weight but not cause birth defects.^{14,15} Mechanisms of 4-chlorophenol photooxidation have been explored previously.¹

In this report, nanocrystalline bismuth vanadate loaded with varying weight percentages of gold nanoparticles were explored in terms of their photocurrents at various potentials and with and without visible-light irradiation. A limited number of 4-chlorophenol degradation experiments were run, and recommendations for future experiments were made. Ultimately, this study will improve the understanding of the photoelectrocatalytic degradation of 4-chlorophenol on a metal oxide support enhanced by gold nanoparticles.

Chapter 2: Background

Much of the early semiconductor photocatalysis research focused upon the use of titanium dioxide (TiO_2), which has been investigated quite thoroughly in photocatalytic and mechanistic studies^{1, 2, 5-12, 16-18} since its discovery in applications of water electrolysis with TiO_2 by Fujishima and Honda.¹⁹ In recent years, alternative photocatalysts have come of interest and many papers on the synthesis and characterization of bismuth vanadate (BiVO_4) can be found.^{4, 5, 13, 20-32} Of these, many have studied the effects of loading transition metals such as gold, platinum, iridium, cobalt, and silver onto TiO_2 and BiVO_4 , with indications that the photocatalytic activity is greatly enhanced.^{2, 3, 6, 8, 9, 20, 22, 23}

2.1 Motivation for Semiconductor Photocatalysis

Semiconductor photocatalysis has been applied to water splitting,^{13, 25} electricity production,³ self-cleaning films, oxidation of gaseous and dissolved organic pollutants, biomass conversion to H_2 and CO_2 ,¹⁷ and selective oxidation reactions of interest to the bulk commodity industry² as well as the photodestruction of cells, bacteria, and viruses.¹⁷ Among the many reactions for which semiconductor photocatalysis has been applied, those related to pollution abatement and organic waste degradation have garnered a large amount of interest in the research community. General types of hazardous wastes include solvents, halogenated hydrocarbons, pesticides, volatile organics, phenols, and dyes.^{1, 4, 17} 4-chlorophenol, the probe compound in this project, is a skin and eye irritant that is toxic if ingested.¹⁴ It is created in the production of pesticides, chlorination of drinking water, and synthesis of dyes and drugs.¹⁸ Groundwater contamination is the primary source of human contact, and numerous studies have explored 4-chlorophenol as a model compound.^{11, 12, 18}

Many of these organic contaminants can penetrate environmental barriers and enter groundwater wells or surface wells after being released in wastewater effluents from industries or households. Military as well as commercial installations have disposed chemical wastes in underground storage tanks and dump sites that eventually contaminate the surrounding soil and groundwater aquifers. This slows the conversion of these facilities to civilian or other uses and cost billions of dollars and take years to cleanup.^{1, 17}

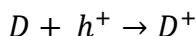
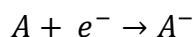
Semiconductor photocatalytic degradation reactions can serve as alternative or complementary processes to more traditional approaches to chemical waste elimination, such as

incineration, anaerobic digestion, activated sludge digestion, and conventional physicochemical treatments.¹ Common water treatment technologies adsorb organic pollutants on activated carbon or utilize air stripping, which do not destroy the contaminants, and incineration is negatively perceived, limiting its use.¹⁶ Therefore, complete mineralization of organic pollutants to CO₂ and inorganic acids is desirable; with wide bandgap semiconductors that have high oxidation potentials under photoexcitation, this is achievable.

2.2 Basics of Semiconductor Photocatalysis

Photocatalysis refers to two distinct mechanisms of catalysis. In one conceptualization of it, it is the acceleration of a photoreaction in the presence of a catalyst whereby the adsorbed substrate absorbs light. In the context of this report, it is photogenerated catalysis, whereby the catalyst itself absorbs light and its photocatalytic activity depends on its ability to create electron-hole ($e^- h^+$) pairs. Creation of electron-hole pairs leads to generation of free radicals (such as hydroxyl radicals) that are able to undergo secondary reactions.¹⁷

In photocatalysis, light acts as an electron pump; atomic or molecular absorption of a photon pumps an electron from an almost full valence band to a nearly empty conduction band. To cause such a transition, the wavelength of light must be with energy equal to or greater than the bandgap, the difference in energies of the two orbitals or bands. This excitation results in an electron ($e^- h^+$) pair. This pair can separate such that the e^- transfers to an acceptor species, A, and the h^+ is filled with an electron from a donor species, D:



If the electron is pumped through a wire and the above redox reactions are separated, useful electrical current can be extracted.^{11, 12} The excited state of charge separation is typically very short-lived and the charge pairs frequently recombine quickly, emitting heat.^{1, 2, 17} Promotion of this separation occurs by introduction of an electric field (when an electrical potential bias is created) or a difference in chemical potential (which occurs when A and D are present). Semiconductor immersion in a solution results in charge transfer at the interface due to the difference in electron affinities between the two phases. An electrical field to a depth on the order of one to several hundred nanometers is created by this difference. In an n-type semiconductor, some electrons are in

the conduction band, so the field is directed from the bulk of the semiconductor to the interface.²⁸ Photogeneration of an $e^- h^+$ pair in this region results in their separation because the electron would move towards the bulk of the semiconductor while the hole would move towards the surface.

A photoelectrochemical cell, as shown in Figure 1, can harness this separation. Species D has an energy level above that of the photogenerated hole at the surface and transfers an electron to fill it, oxidizing D. The excited electron is transferred through a wire connected to the semiconductor or a conductive substrate on which it is backed to an inert counter electrode and reduces species A. The overall reaction in this cell comprised of the n-type semiconductor, nonphotoactive electrode, and electrolyte is:

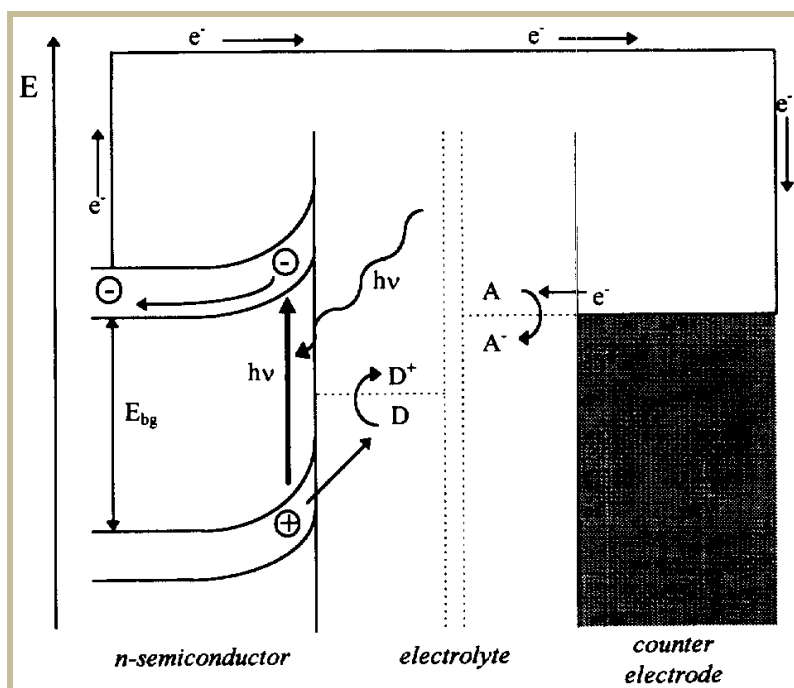
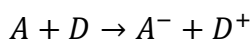


Figure 1: Basic schematic of a photoelectrochemical cell with an n-type semiconductor. Note that band bending is indicated. Electrons move spontaneously downhill and holes uphill. Adapted from [17].

An external electrical source would drive the reaction in the uphill direction in addition to the electron pump provided by the light. The photoelectrochemical cell provides on its own the required field for $e^- h^+$ separation as well as the special distance between the products of the photoredox reaction, which could potentially react with each other.

Figure 2 summarizes the processes involving $e^- h^+$ pairs upon photoexcitation of a semiconductor particle by light greater than the bandgap of the semiconductor. Upon generation and subsequently separation of the charge pairs, competing processes can occur. Deactivation and degradation of light energy into heat occurs with recombination of the charges at the surface (path A) or in the bulk (path B). After diffusing to the surface, interfacial electron transfer occurs. Photogenerated electrons reduce the electron acceptor (path C), and photogenerated holes oxidize the electron donor (path D). In a photoelectrochemical cell, the electrons would be drawn through the wire and react at the surface of the counter electrode. The combination of the reactions given by path C and path D is the overall redox reaction that can occur in the cell.

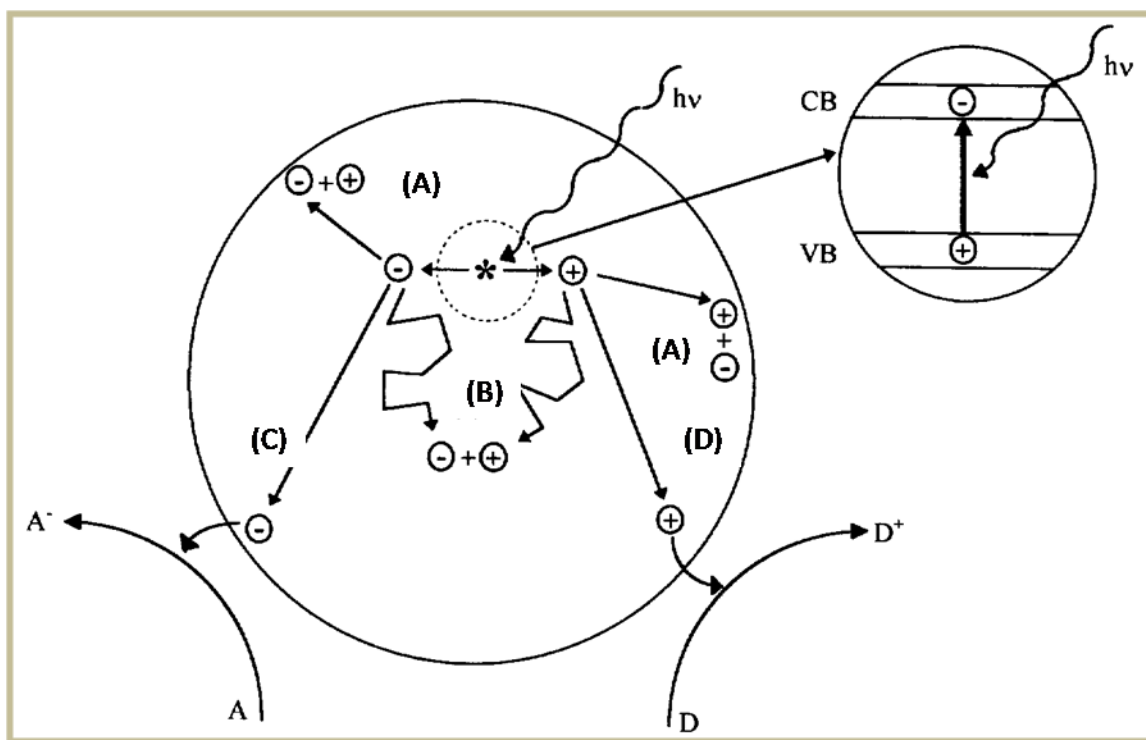


Figure 2: Schematic of major processes following $e^- h^+$ photogeneration. Adapted from [17].

From laser flash photolysis experiments, primary processes associated with the mineralization of organic compounds via heterogeneous photocatalysis over TiO_2 were identified, along with their characteristic time domains, shown in Table 1. $>TiOH$ is the primary hydrated surface functionality of TiO_2 . The organic compound acts as an electron donor while oxygen is an electron acceptor. Typically, the organic does not undergo direct hole transfer but rather is oxidized by a surface-bound hydroxyl radical. A full kinetic model for these sets of reactions is difficult to establish and may vary depending upon the substrate used.

Primary process	Characteristic time
Charge carrier generation $\text{TiO}_2 + h\nu \rightarrow \text{h}^+ + \text{e}^-$	fs (very fast)
Charge carrier trapping $\text{h}^+ + >\text{Ti}^{\text{IV}}\text{OH} \rightarrow \{>\text{Ti}^{\text{IV}}\text{OH}^+\}$ $\text{e}^- + >\text{Ti}^{\text{IV}}\text{OH} \leftarrow \{>\text{Ti}^{\text{III}}\text{OH}\}$ $\text{e}^- + >\text{Ti}^{\text{IV}} \rightarrow >\text{Ti}^{\text{III}}$	10 ns (fast) 100 ps (shallow trap; dynamic equilibrium) 10 ns (deep trap)
Charge carrier recombination $\text{e}^- + \{>\text{Ti}^{\text{IV}}\text{OH}^+\} \rightarrow >\text{Ti}^{\text{IV}}\text{OH}$ $\text{h}^+ + >\text{Ti}^{\text{III}}\text{OH} \rightarrow >\text{Ti}^{\text{IV}}\text{OH}$	100 ns (slow) 10 ns (fast)
Interfacial charge transfer $\{>\text{Ti}^{\text{IV}}\text{OH}^+\} + \text{organic pollutant} \rightarrow >\text{Ti}^{\text{IV}}\text{OH} + \text{oxidized pollutant}$ $\{>\text{Ti}^{\text{III}}\text{OH}\} + \text{O}_2 \rightarrow >\text{Ti}^{\text{IV}}\text{OH} + \text{O}_2^-$	100 ns (slow) ms (very slow)

Table 1: Processes and characteristic times in TiO_2 photomineralization of organics. Adapted from [1, 17].

Two popular photocatalysts are TiO_2 , which has a bandgap of 3.2 eV in its anatase form,^{5, 8} and BiVO_4 , with a bandgap of 2.4 eV.^{5, 13, 24} Numerous others have also been studied and most are metal-oxide systems, with different bandgaps and spectrums in which they are photoactive, including ZrO_2 , SiO_2 , doped forms of TiO_2 , zeolites, CdS, ZnO, Fe_2O_3 , and WO_3 .^{2, 17} Wide band gap semiconductors such as the commonly studied TiO_2 are in general not photocatalytic under visible light, which would be a requirement for efficient solar energy utilization.²² Consequently, materials capable of photoinduced charge separation upon excitation in the visible spectral region have garnered intense interest.

Bismuth vanadate exhibits catalytic photooxidation activity and promising photoelectrochemical properties when irradiated at wavelengths less than 520 nm, which corresponds to its bandgap of about 2.4 eV, and thus is suitable for applications using natural or ambient visible light.^{13, 33} Monoclinic BiVO_4 prepared by facile hydrothermal techniques and coprecipitation reactions appears to be the most photoactive morphology for BiVO_4 for a variety of organic degradation reactions.^{4, 5, 20, 21, 24, 26, 27, 29-32} Additional requirements for improved photocatalysts are better performance, high energy efficiency, environmental benignity (biological and chemical inertness), low cost, long lifetime and photostability, and the ability to utilize visible and/or near-UV light.^{17, 34}

2.3 Photocatalysts with Metal Nanoparticle Modification

Most research on the modification of metal oxide photocatalysts with metal nanoparticles has investigated Ag/ TiO_2 , Ag/ BiVO_4 , or Au/ TiO_2 . Gold modification of BiVO_4 has so far been quite rare. In all cases, surface modification of the semiconductor with metal nanoparticles accelerated the photooxidation reactions studied. This is mainly attributed to improvement in the charge-transfer

process at the interface of the metal/semiconductor and surface plasmon resonance (SPR). The SPR effect is due to the collective oscillations of the conduction-band electrons in the nanoparticles upon resonance with the electric field of an electromagnetic wave (i.e., the incident light shone upon them).^{2, 6, 9, 10} Zhu, et. al.² determined that visible light absorption by Au nanoparticles attributed to SPR originates from intraband excitation of 6sp orbital electrons while UV light absorption originates from interband excitation of electrons from 5d to 6sp.

Wodka, et al.⁹ report that a common Ag/TiO₂ composite system was able to absorb light in the whole visible region, with the appearance of optical effects in absorbance spectra attributed to the SPR effect. The potential for oxidation of silver is relatively similar to that of the conduction band edge of TiO₂; this allows electrons to flow in both directions and enables capture of a hole by a silver nanoparticle. This potential for gold is much less than the conduction band edge of TiO₂, so the electrons can flow in one direction only; gold nanoparticles deposited at the TiO₂ surface can become traps for electrons, enhancing the charge separation step of the irradiation response. According to Kohtani, et al.,²⁰ oxidation of water by valence-band holes on Ag/BiVO₄ surfaces generates OH radicals, which greatly contributes to organic degradation.

Chandrasekharran, et al.⁸ determined that Au particles adsorbed on TiO₂ films were larger in diameter (50 – 70 nm) than particles in solution (5 nm) but still retained similar surface plasmon characteristics. They found a 3-fold enhancement in photocurrent generation due to the Au nanoparticles and explained this increased efficiency by the promotion of charge separation within the nanostructured TiO₂ network and of the interfacial charge-transfer process. A schematic illustrating the mechanism of these improved charge transfer kinetics is shown in Figure 3. Tian et al.¹⁰ explain that Au nanoparticles are photoexcited due to SPR, and charge separation occurs by the transfer of photoexcited electrons from the Au particle to the TiO₂ conduction band and simultaneously by the transfer of electrons from a donor in the solution to the gold particle. The electrons injected into the TiO₂ conduction band can then be drawn through a wire and transferred to O₂ or another electron acceptor elsewhere in the photoelectrochemical cell.

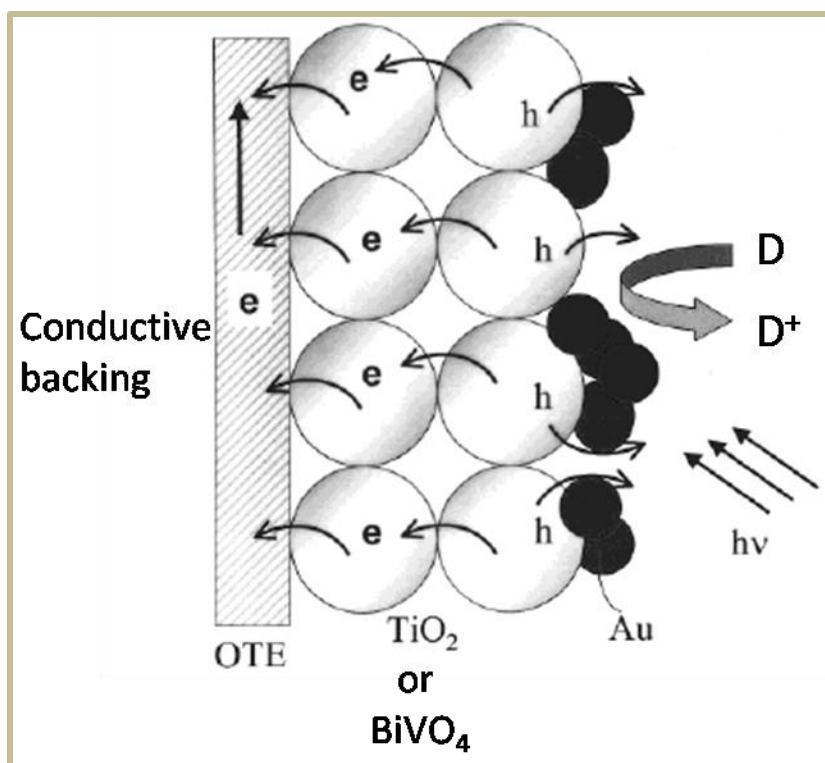


Figure 3: Charge separation in a TiO_2 or BiVO_4 electrode on optically transparent electrode modified with gold nanoparticles upon irradiation and presence of a redox couple. Adapted from [6, 8].

Charge separation at a plasmon-excited metal nanoparticle is accompanied by corrosion or degradation of the particle.¹⁰ Subramanian, et al.⁶ caution that photocurrent measurements and photocatalytic degradation experiments employ different experimental conditions, related to the length of illumination time. Photocurrents are measured using short-term illumination, while degradation involves long-term illumination; deterioration of the metal/semiconductor interface during long-term operation of a photoelectrode likely limits the benefits of metal nanoparticle deposition. In composite films, the oxidation of the metal nanoparticles in the presence of oxidizing radicals and valence-band holes disrupts the metal/semiconductor interface but also creates new electron-hole recombination centers, such as Au^+ . Some of these metal ions diffuse into the photocatalyst matrix but many recombine with photogenerated electrons, reducing the efficiency in a net loss of electrons. Contributions by these recombination centers are negligible for short-term irradiation, but continued irradiation could become detrimental to photocurrent generation.

Chapter 3: Methodology

The overall procedure was as follows. The catalyst powder was mixed into a slurry of ethyl cellulose, ethanol, and terpineol. This paste was doctor bladed onto the conductive side of FTO glass pieces to form the electrode; these electrodes were then heated in a furnace. The calcined electrodes were assembled into an electrochemical cell, with the catalyst side contacting the electrolyte solution and the other side exposed to irradiation from a xenon lamp. Various experiments could be performed with or without irradiation and/or filters while potential and current through the electrochemical setup and time could be recorded and plotted. The electrolyte was sodium sulfate with 4-chlorophenol and, in a few runs, hydrogen peroxide added. The 4-chlorophenol samples were analyzed in a UV-vis spectrometer. All potentials were measured versus the potential of the Ag/AgCl reference electrode saturated with KCl (+0.197 V vs. NHE, normal hydrogen electrode). All water used for preparation of solutions and cleaning of glassware was purified by a Hitech-Kflow reverse osmosis deionization (RO DI) water purification unit that provided water with a resistivity up to 15 M Ω -cm. Gloves, safety glasses, and a lab coat were worn throughout the duration of all experiments and handling of chemicals. Data from the photoelectrochemical experiments was collected by the potentiostat software and then converted to a text format. These text files were imported into OriginLab 7.5 and Microsoft Office Excel 2007 for graphing and analysis.

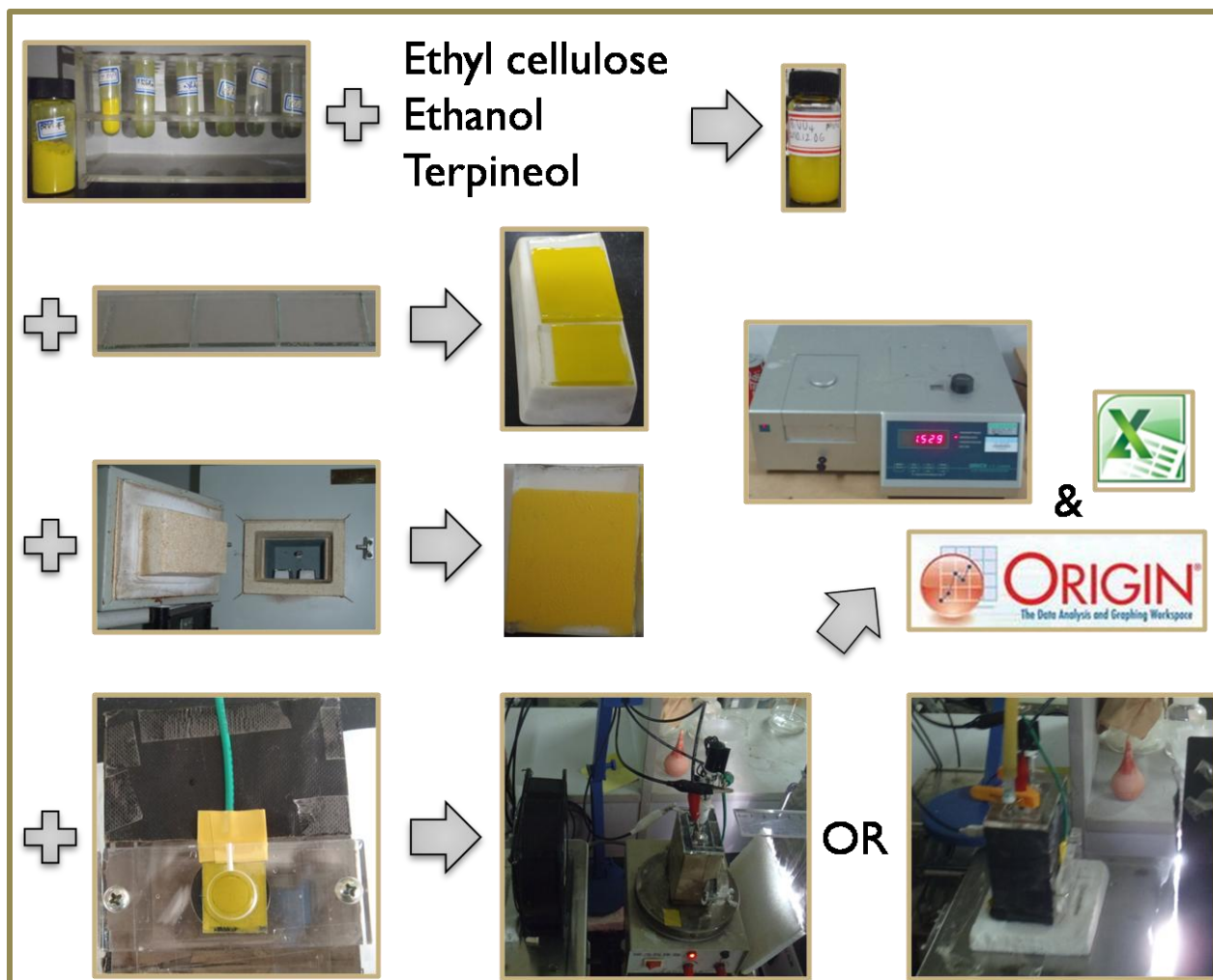


Figure 4: Schematic of the overall methodology

3.1 Synthesis of Catalyst Paste

Monoclinic BiVO_4 powders were synthesized according to the description of Kohtani, et al.^{4,5} Aqueous equimolar $\text{Bi}(\text{NO}_3)_3$ and NH_4VO_3 solutions (0.4 M) containing HNO_3 (1.84 M) were prepared separately. After 100 mL each of these two solutions were mixed, 7.5 g of urea was added. The mixed solution was then stirred at 90°C for eight hours. The BiVO_4 precipitation formed by the hydrolysis was washed by water, filtered, and dried at 45°C .

The bismuth vanadate was modified with gold nanoparticles using a gold precursor of chloroauric acid (HAuCl_4). The preparation was performed by deposition-precipitation with urea. Usually, BiVO_4 powder (1 g) was dispersed into 0.42 M urea solution with a desirable amount of HAuCl_4 aqueous solution (4 g/100 mL water) was added to achieve the desired gold content (0.5

wt%, 0.75 wt%, 1 wt%, 2 wt%, or 4 wt%). This suspension was sonicated for 30 minutes and then stirred in a water bath at 90°C for four hours in a sealed flask. The resulting precipitate was collected, washed with water, and dried. Finally, Au/BiVO₄ was obtained by calcinations at 300°C for two hours.

To prepare a paste of the appropriate powder, ethyl cellulose (0.2 g) was mixed into ethanol (2 mL) over five minutes. The catalyst powder (1 g) was added along with terpineol (1 mL) and the resulting mixture was mixed for another five minutes using a glass stirring rod.

3.2 Preparation of FTO Glass Electrode

Fluorine-doped tin oxide coated glass (FTO glass), a transparent and conductive substrate, was used as the catalyst support and electrode. The conductive side was identified by a finite reading by a multimeter on a resistance setting. Electrodes were measured into the appropriate dimensions with a ruler and then scored once on the nonconductive side at the correct intervals with a diamond-edge cutter. They were separated by placing the small end between two stiff, flat surfaces and snapping off the larger end. The electrodes were handled with plastic tweezers and placed into separate covered weighing dishes and cleaned. They were sonicated in water and soap for ten minutes, then again in ethanol, and once more in acetone, with triple rinses with water in between each sonication step. The electrodes were then dried under an infrared lamp.

The thin film electrode was prepared by doctor blading the catalyst paste onto the conductive substrate of the electrode with a glass stirring rod. A thin strip at the top of the electrode was left bare so that a copper wire could be attached to create the working electrode in the electrochemical setup. It was necessary to calcine the electrodes in order to remove the volatile organics and promote the adsorption of the catalyst film on the FTO glass. The electrodes were calcined in alternating periods of temperature ramps and of constant temperature. The rate of temperature change was 5°C/min, and the calcinations program lasted 305 min, or about 5 hours. The temperature-time profile is shown in Figure 5. Figure 6 shows BiVO₄ electrodes before and after calcination.

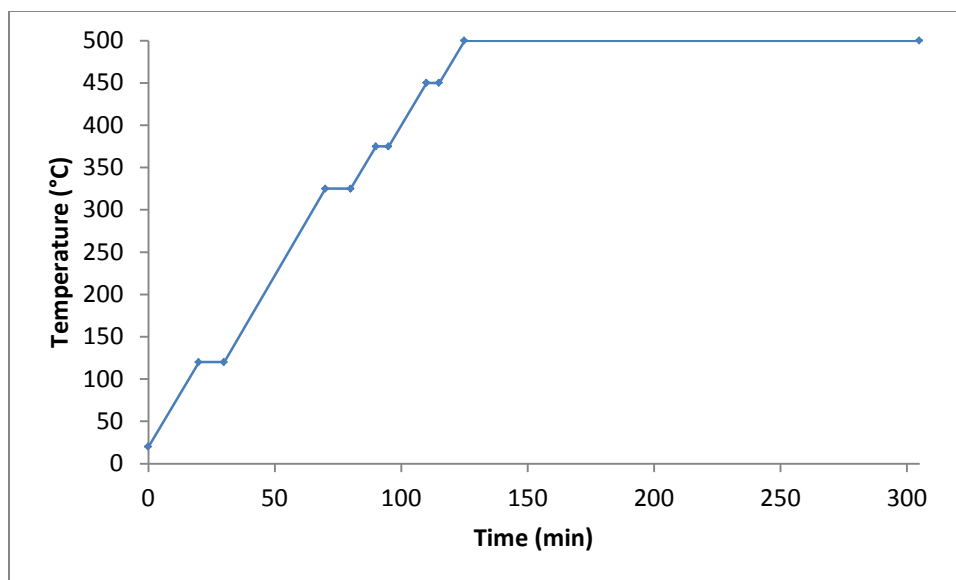


Figure 5: Temperature-time profile of the electrode calcination program

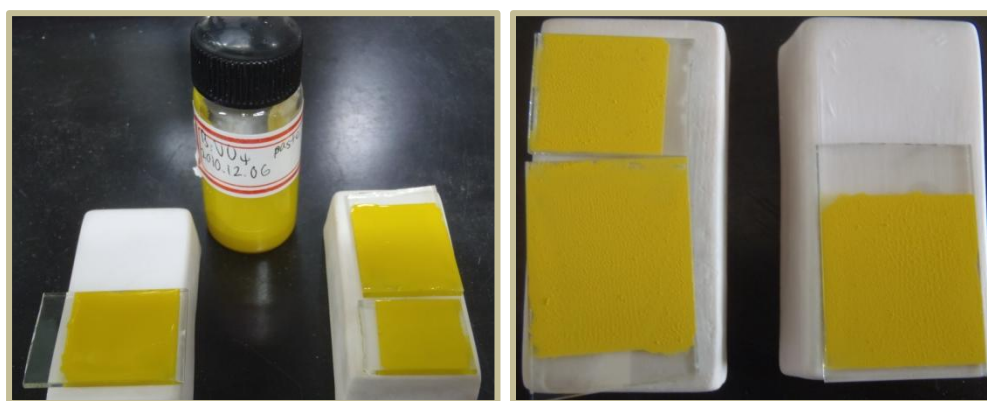


Figure 6: Left: Bismuth vanadate in a vial and doctor bladed on three FTO glass electrodes; right: the same electrodes after calcination.

3.3 Assembly of Electrochemical Cell

The electrochemical cell was made of plastic with a removable top and a circular opening towards the bottom of the front. The cell was covered in construction paper to limit the exposure of light to the contents. The top had ports for the counter electrode, reference electrode, and gas bubbler. The working electrode (FTO glass) was sandwiched between an O-ring in the groove around the front opening and a plastic plate that could be secured and tightened by screws or wingnuts. The electrode and openings in the cell and the plate were aligned so that the catalyst layer in contact with the electrolyte solution would be exposed to light irradiated from a xenon lamp with an infrared filter to avoid overheating.

Once the electrode was secured in place, the electrochemical cell was filled with the appropriate electrolyte solution; care was taken not to create bubbles in the channel in front of the working electrode. The cell was covered with its top, and the reference electrode, Ag/AgCl saturated with KCl, and the counter electrode, Pt wire, were inserted into the cell. If necessary, a syringe needle connected to a gas line was inserted into the cell in order to sparge nitrogen into the electrolyte solution. The cell was placed onto a stand with an adjustable height in front of a 500-W xenon lamp at a distance of 10 ± 0.1 cm, measured from the front filter of the lamp to the center of the working electrode. The electrodes were connected to the potentiostat by wires with alligator clips.

Two different electrochemical cells were used. When the electrodes were being characterized in 0.5 M Na_2SO_4 , a larger cell with a front hole of area 0.785 cm^2 , was used. However, when 4-chlorophenol degradation experiments were carried out in 0.5 M Na_2SO_4 and 10 mg/L 4-chlorophenol, a smaller reactor with a larger opening in the front, of area 1.77 cm^2 , was found necessary. The xenon lamp was always operated at 20.0 A, and a cooling fan was directed at the cell in order to prevent significant heating.

Upon completion of experiments with the electrochemical cell, it was disassembled and all parts and electrodes were triple rinsed with water. It was found that a white precipitate would form if the electrolyte solution was left in the cell.

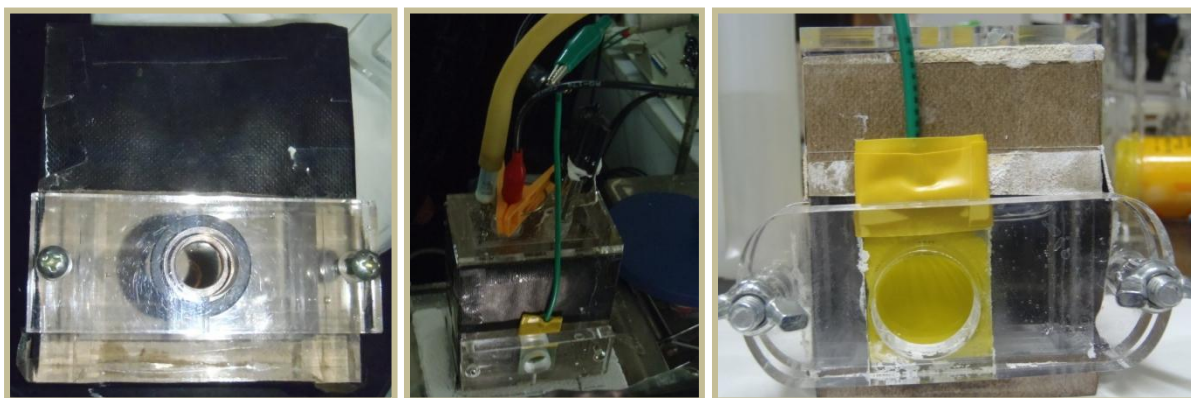


Figure 7: Pictures of the electrochemical cell. From left to right: The large electrochemical cell with no electrodes; the same cell fully assembled; the small cell with a bismuth vanadate electrode in place after the electrolyte was left to sit in the cell overnight.

3.4 Characterization

The filters used were 420 nm, 490 nm, 535 nm, 600 nm. The 535 nm and 600 nm are above the wavelengths of light absorbed by bismuth vanadate, so any activity observed should be due to the gold nanoparticles. When the platinum-wire counter electrode was replaced by a graphite electrode or when the FTO glass was pre-treated with TiCl_4 (to reduce background noise), there were no significant changes in the photocurrent measurements. When a potential is applied, there is usually a built-in delay before the current is recorded in order to allow the system to equilibrate.

3.4.1 Linear Sweep Voltammetry

In linear sweep voltammetry (LSV), an initial potential is applied and then increased linearly at a constant rate until a final potential is reached. The current is recorded, and current versus potential graphs are generated. All linear sweep voltammograms were generated in 0.5 M Na_2SO_4 by sweeping from -0.5 V to 1.2 V (vs. Ag/AgCl) with a scan rate of 0.05 V/s after an initial two second delay and with data recorded every 0.001 V at a sensitivity of 0.001 A/V. For a given sample and filter, an LSV was produced with no illumination (“dark” LSV) and then with irradiation. The dark LSV indicates the level of background current present in that experimental setup; the illuminated LSV should be compared to the dark LSV to determine the level of photocurrent induced by the illumination. For one sample, BiVO_4 , a cyclic voltammetry (CV) was performed; it scanned between -0.5 V and 0.5 V (vs. Ag/AgCl) with the other settings identical to those for the LSVs. The CV swept forward and backward for 10 cycles.

3.4.2 Chronoamperometry

In chronoamperometry (CA), a constant potential is applied and the transient photocurrent is measured over time. This was performed in 0.5 M Na_2SO_4 under chopped irradiation of unfiltered visible light from the xenon lamp in order to elucidate information on the rates of the electron-hole transfer processes. By removing an aluminum shield in front of the lamp, the cell was irradiated for 5 seconds. After irradiation, the lamp was again shielded. The potentials that were probed were 0.2 V, 0.5 V, -0.2 V, and -0.4 V (in that order), with a sensitivity of 0.001 A/V and sample interval of 0.001 s after an initial delay of five seconds.

3.4.3 Degradation of 4-Chlorophenol

Degradation of 4-chlorophenol was carried out in a solution of sodium sulfate and 4-chlorophenol. Solutions were prepared from a stock solution of 1 g/L 4-CP and 1 M Na₂SO₄. In the case where 5 mM or 10 mM H₂O₂ was also present in the solution, a 0.1 M H₂O₂ stock solution was used. The small electrochemical cell was thus filled with 40 mL of 0.5 M Na₂SO₄, 20 mg/L 4-CP, and 0, 5, or 10 mM H₂O₂. A constant potential of 1.0 V (vs. Ag/AgCl) was applied through a one-hour long chronoamperometry program under constant irradiation. For one sample of BiVO₄, another program was tested: applied -0.2 V for 300 s and then 1.0 V for 900 s and repeated this cycle 3 times per hour. At the hour, the lamp was shielded, and an approximately 1.5 mL sample was drawn off from the solution using a syringe that was thoroughly washed between uses. These samples were stored in labeled vials in a dark refrigerator to be tested later. Then this process was repeated for a total of four hours of degradation. The experimental setup is displayed in Figure 8.

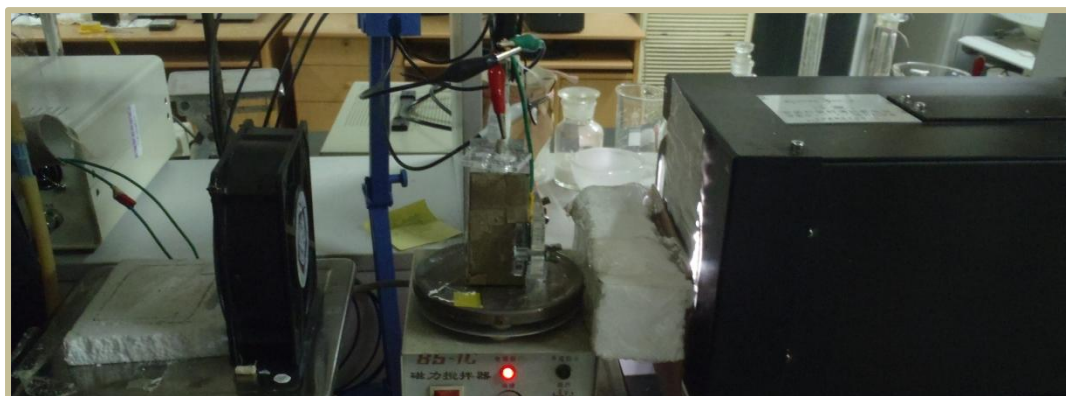


Figure 8: The experimental setup for 4-chlorophenol degradation.

Immediately following the completion of the experiment, the absorbance of each sample was taken in a quartz cuvette against a blank of 3 mL of 0.5 M Na₂SO₄. The absorbances over the wavelength range of 200 nm to 700 nm were determined, with the region 210 nm to 310 nm being the most important to features exhibited by 4-chlorophenol. The strongest peaks can be seen at 230 nm and 280 nm.

3.4.4 SEM

Surface morphology was imaged by scanning electron microscopy. Due to limited time, SEM images were taken only for one of each of the following: 0 wt%, 0.5 wt%, 1 wt%, and 2 wt% Au/BiVO₄. These were recorded at various magnifications 200-200000x, as shown in Table 2, with an accelerating voltage of 5.00 kV on a FEI Sirion 200 Field Emission SEM.

Table 2: Magnifications of SEM images for 0, 0.5, 1, and 2 wt% Au/BiVO₄.

Sample	BiVO ₄	0.5 wt% Au/BiVO ₄	1 wt% Au/BiVO ₄	2 wt% Au/BiVO ₄
Available Magnifications	200	200	500	200
	500	1000	1000	1000
	10000	10000	2500	50000
	40000	100000	5000	100000
	50011		9000	200000
			10000	
			20000	
			40000	

Chapter 4: Results and Discussion

The bismuth vanadate powders were yellow; when they were modified with gold, the resulting powder was green but had the same texture. During the synthesis of the catalyst paste and the preparation of the electrode, care was taken to prevent it from agglomerating and forming bumps in the thin film on the FTO glass. Samples were prepared in duplicate, so electrodes with visibly rough surfaces were not used. After the calcination of the electrode, they were placed into the electrochemical cell and linear sweep voltammetry and chronoamperometry were performed. Following this, select electrodes were employed in 4-chlorophenol degradation and then characterized by scanning electron microscopy. Figure 9 shows the different electrodes investigated.

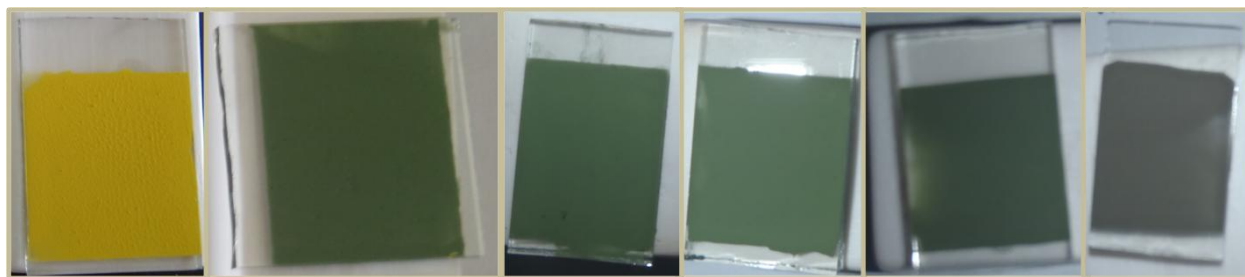


Figure 9: The working electrodes after calcination coated with a thin film of (from left to right) 0 wt%, 0.5 wt%, 0.75 wt%, 1 wt%, 2 wt%, or 4 wt% Au/BiVO₄.

4.1 Linear Sweep Voltammetry

In Figure 10, each black curve is a linear sweep voltammetry (LSV) under dark conditions – the xenon lamp was shielded with an aluminum plate. There was some variation among the repeated dark curves due to errors in the potentiostat measurement and possibly due to changes in the electrode as they are used. The colored curves were LSVs performed with illumination. For each electrode, the data appeared to be inconclusive as to the effect that gold has, considering the 535 nm and 600 nm filter. However, a clear trend could be observed with the other filters. The red curve demonstrated that there was significantly more activity for positive potential biases when the catalyst was illuminated with light with no filter than when there was no illumination. The green curve indicated that some of the photocatalytic activity is reduced when light with wavelengths shorter than 420 nm is filtered. As seen with the blue curve, this trend continued with the 490 nm filter, as only a small amount of activity observed at higher positive potentials. The 535 nm and 600 nm filters cut off any significant activity above the background.

In the case of (Figure 10A), this was to be expected as the bandgap of BiVO_4 corresponds to a wavelength of about 520 nm. Filtering light below this wavelength would inhibit the generation of electron-hole pairs necessary for BiVO_4 to be photoactive and conduct current. The other charts in Figure 10 show the results of linear sweep voltammetry with the gold-modified BiVO_4 electrodes. A major difference between these LSVs and those with BiVO_4 was that a cathodic current was more readily achieved. With no filter and with a 420 nm filter and below ~ 0 V vs. Ag/AgCl, the current was less than the dark currents. However the trend of the magnitude of the photocurrents at a given potential at the extreme potentials was still the same: no filter > 420 nm filter > 490 nm filter > 535 nm filter > 600 nm filter. The 535 nm and 600 nm curves were always very similar to the dark curves, calling into question whether the ability of gold to provide activity above these wavelengths can be determined by these methods. The magnitudes of the current densities achieved should only be qualitatively compared because the densities were determined from geometric area, not the true catalytic surface area, which was not determined due to limited time.

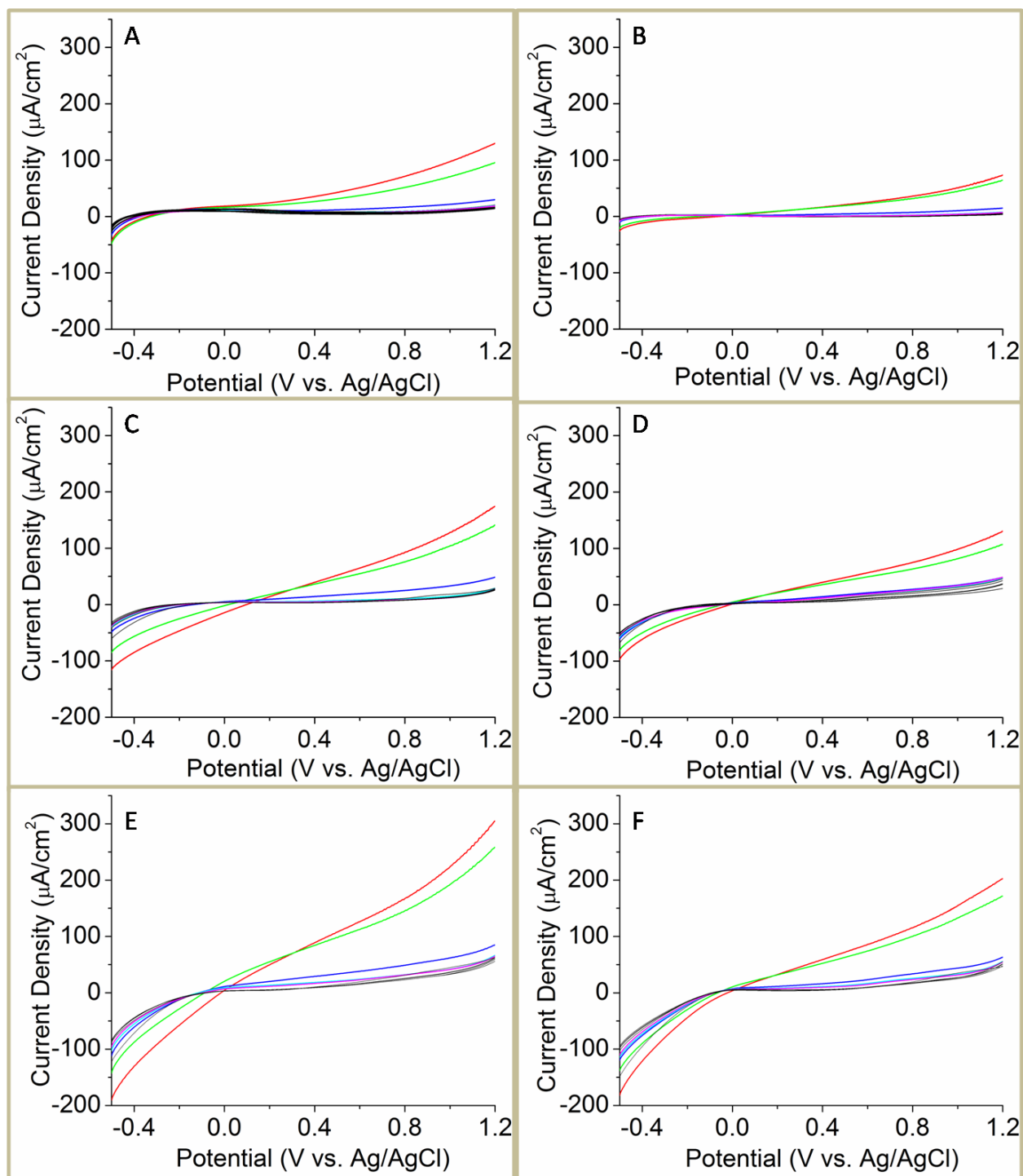


Figure 10: Linear sweep voltammetry from -0.5 V to 1.2 V (vs. Ag/AgCl) for (A) BiVO_4 , (B) 0.5 wt% Au/ BiVO_4 , (C) 0.75 wt% Au/ BiVO_4 , (D) 1 wt% Au/ BiVO_4 , (E) 2 wt% Au/ BiVO_4 , and (F) 4 wt% Au/ BiVO_4 and (black) without illumination and with irradiation filtered in the following manner: (red) no filter, or (green) 420 nm, (blue) 490 nm, (cyan) 535 nm, or (magenta) 600 nm filters. Note that the 535 nm and 600 nm results are indistinguishable from the background. The non-illuminated curves were generated several times to test reproducibility. The current density is calculated as the current divided by the area of the electrode exposed to the electrolyte solution, 0.785 cm^2 .

Out of interest to test the stability of the BiVO_4 , a cycle voltammogram (CV) from -0.5 V to 0.5 V vs. Ag/AgCl was obtained before the chronoamperometric photocurrent measurements, shown in Figure 11. The red curve demonstrates that the photocurrent is relatively stable under dark conditions. However, the blue curve indicates that the photocurrent changes with time under illuminated conditions; this is because the illumination is effectively inducing the separation of charges and holes, and electrons are being depleted. The CVs in both cases demonstrate hysteresis as the forward scan is not the same as the backward scan.

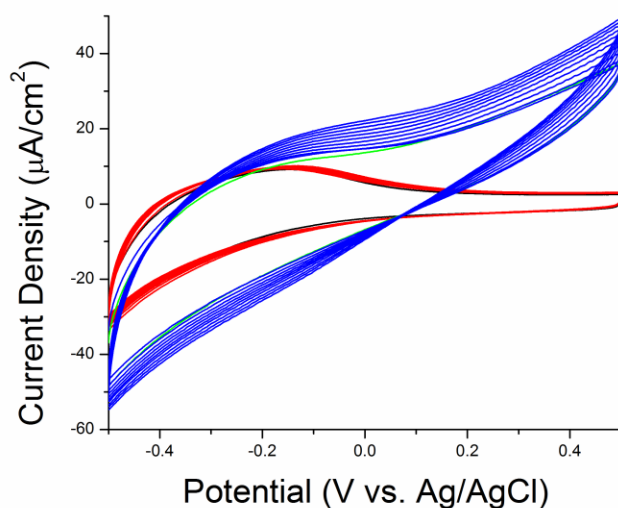


Figure 11: CVs performed with BiVO_4 electrode before photocurrent measurements. The red curve (and black curve that it overlaps) were obtained in dark conditions. The blue curve (and green curve that it overlaps) were obtained in illuminated conditions.

4.2 Chronoamperometry

Figure 12 plots the results of chopped irradiation chronoamperometric photocurrent measurements, whereby a given potential was applied, the lamp was unshielded and then shielded, and the current measured as it varies with time. The start of the region of interest is when the catalyst is illuminated and the end of it is when the lamp is shielded. The response can be indicative of the mechanism of electron-hole pair generation. Differences between these responses among the different catalysts being studied would indicate a change in preferred routes. The magnitude of the current density in this region is indicative of the amount of catalytic activity. Because the data was generated over periods of time that were not exactly identical and the general shape of the curve is independent of absolute time, the time scale is not explicitly shown; the timescale for each run was

adjusted so that the time when the lamp was unshielded (a spike in current is observed) were approximately uniform. The chronoamperometric photocurrent measurements obtained when a filter was occasionally applied followed the same trend as for the LSVs when a filter was applied; that is, the same generic shape was retained but the magnitude of the response was diminished.

For 0, 1, and 4 wt% Au/BiVO₄, the curves at each potential were very similar in magnitude and in shape. Potentials of 0.5 V and 0.2 V resulted in anodic (positive) currents, with that at 0.5 V higher than at 0.2 V. At -0.2 V and -0.4 V, the current was cathodic (negative), with that at -0.2 V only marginally more positive than that at -0.4 V. The 2 wt% Au/BiVO₄ exhibits much greater magnitudes of photocurrent densities, especially at 0.5 V and -0.4 V. This demonstrates that a 2 wt% loading of gold onto bismuth vanadate greatly enhances its photoactivity and may be the most interesting catalyst to employ in the working electrode for the 4-chlorophenol degradation experiments.

As seen in Figure 12B and Figure 12C, the features for the curves representing 0.5 wt% and 0.75 wt% Au/BiVO₄ were similar to those for BiVO₄ at 0.5 V, -0.2 V, and -0.4 V. However, the response at 0.2 V was cathodic (the current density is negative) instead of anodic (positive). This indicates that a cathodic current was produced more readily or easily on the gold-modified BiVO₄ than with the unmodified form. The gold nanoparticles scavenged the electrons generated during electron-hole pair separation on the photocatalyst and facilitated the conduction of the electrons to the electrolyte. Since the solution was bubbled with nitrogen, the reduced species was likely water. This conclusion did not always hold for the other electrodes. The chronoamperometric photocurrent at 0.2 V was cathodic when it was anodic for the other gold-modified samples; this was attributed to an effect by gold. However, this may have been due to oxygen diffusing into the solution. For the 1 wt% Au/BiVO₄ sample, a similarly cathodic current was observed at first, but the run was repeated. When the nitrogen purge was increased in flow and the CA was repeated, the current became anodic. The current at 0.2 V was generally small in magnitude, so it would have been sensitive to fluctuations in the concentration of oxygen; trace amounts of oxygen would have driven the current to become more negative (more cathodic). Lack of oxygen, trace gases, and other contaminants may have contributed to the different results. As experiments were performed, the lab technique of the investigator improved and so later data is probably more consistent with the methodology laid out in Chapter 3. Unfortunately, the measurements for 0.5 wt% and 0.75 wt% could not be repeated due to time constraints.

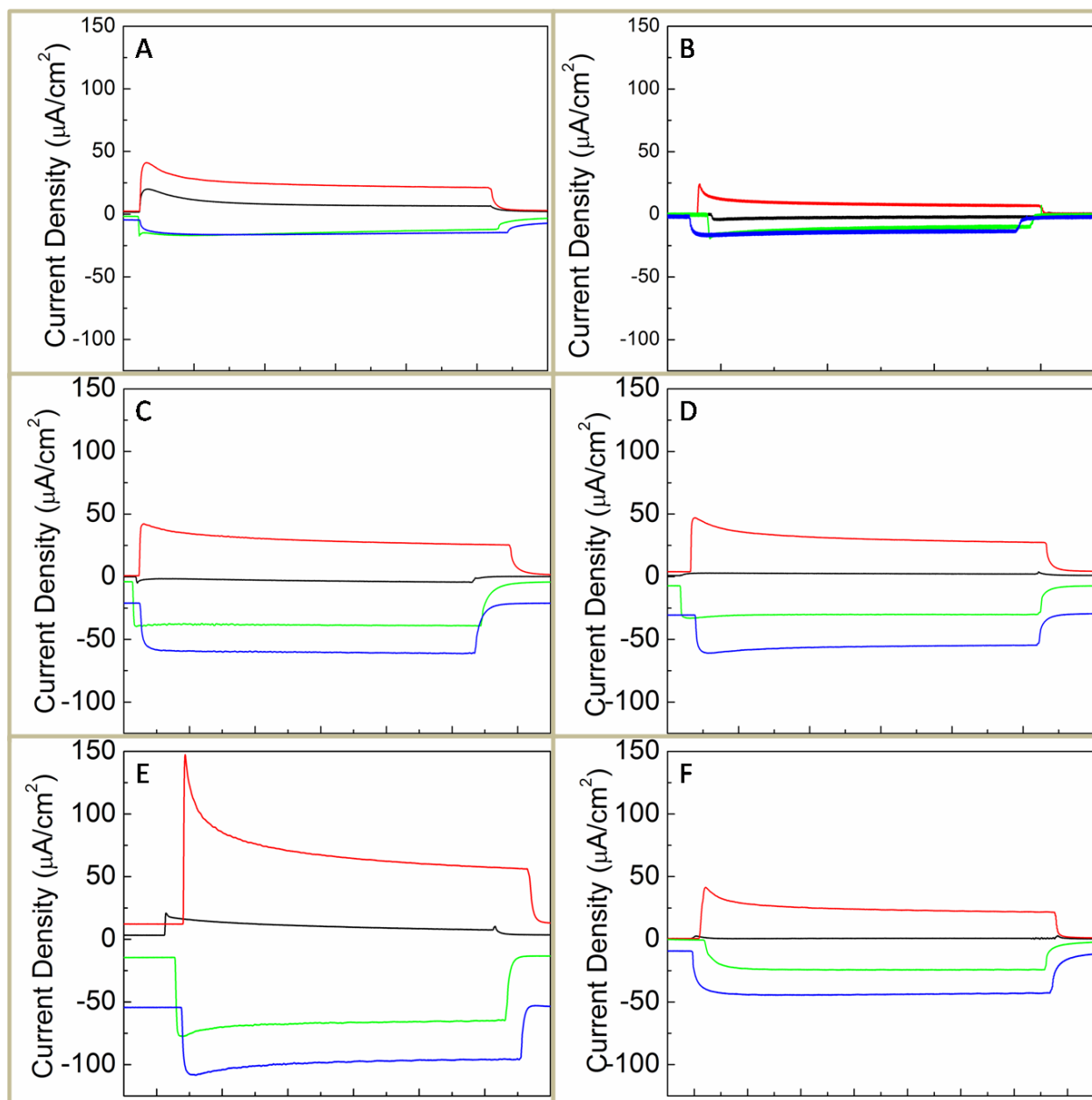


Figure 12: Chronoamperometric photocurrent measurements at constant potentials of (red) 0.5 V, (black) 0.2 V, (green) -0.2 V, and (blue) -0.4 V (vs. Ag/AgCl) for (A) BiVO_4 , (B) 0.5 wt% Au/BiVO_4 , (C) 0.75 wt% Au/BiVO_4 , (D) 1 wt% Au/BiVO_4 , (E) 2 wt% Au/BiVO_4 , and (F) 4 wt% Au/BiVO_4 with illumination and no filters. The current density is calculated as the current divided by the area of the electrode exposed to the electrolyte solution, 0.785 cm^2 .

Figure 13 compares the photocurrent measurements of BiVO_4 and 2 wt% Au/BiVO_4 at 0.5 V with different filters. In each chart, the black curve was obtained with no filter, the red curve was with the 420 nm filter, the green curve with the 490 nm filter, the blue curve with the 535 nm filter, and the cyan curve with the 600 nm filter. It can be seen that for each potential, the photocurrent for BiVO_4 is much smaller than that for 2 wt% Au/BiVO_4 . The currents for the 535 nm and 600 nm

filters appear identical to each other for both electrodes. A small amount of activity is observable for BiVO_4 , but the activity for 2 wt% Au/BiVO_4 is much more significant. No photocurrent density would be expected for the 535 nm or 600 nm filters with BiVO_4 because it is not supposed to absorb above 520 nm. However, there was a small yet noticeable photocurrent with these filters. This may be due to a background capacitance in the solution created because the electrodes in the three-electrode setup were not immediately adjacent to each other in the cell. For 2 wt% Au/BiVO_4 , there was an increased photocurrent density measured with the 535 nm or 600 nm filters applied. One could attribute this to the presence of the gold in the sample. However, this may be caused by the capacitance within the solution being different due to a slightly different experimental setup. Therefore, the effect of gold at wavelengths above 520 nm cannot be conclusively determined.

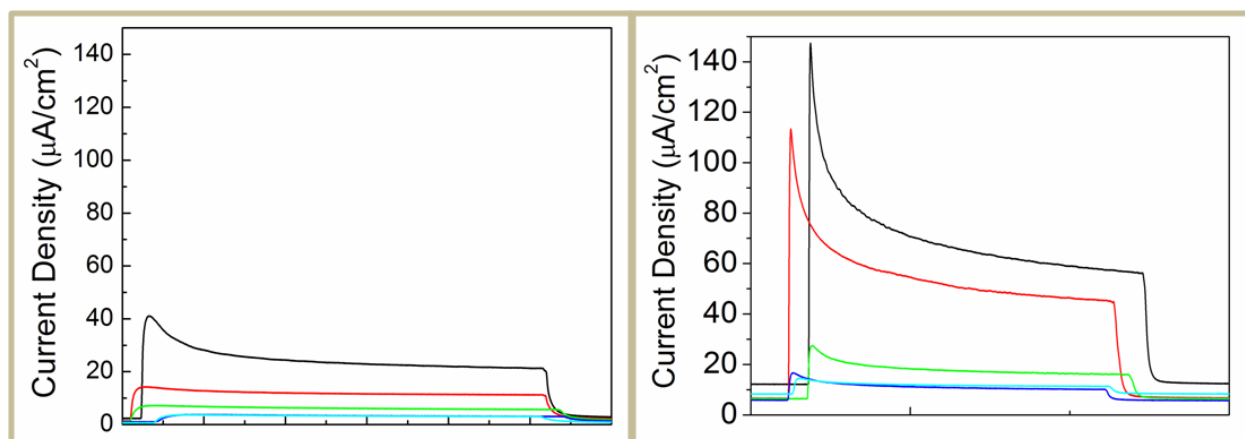


Figure 13: Chronoamperometric photocurrent measurements for (left) BiVO_4 and (right) 2 wt% Au/BiVO_4 at 0.5 V with different filters: (black) no filter, (red) 420 nm, (green) 490 nm, (blue) 535 nm, and (cyan) 600 nm.

4.3 Degradation of 4-Chlorophenol

From the photocurrent measurements, it was decided that 2 wt% Au/BiVO_4 showed the most activity; photodegradation experiments were also done with BiVO_4 . The two different degradation programs used with BiVO_4 were: 1.0 V constant applied potential; apply -0.2 V for 300 s and then 1.0 V for 900 s and repeat this cycle 3 times per hour. The logic behind the second program is that applying a cathodic potential of -0.2 V should restore the electrons in the photocatalyst and should decompose any peroxide generated on the surface of the electrode at the high anodic bias of 1.0 V. However, the absorbance readings did not improve appreciably, so the first program was utilized in subsequent runs. With the constant applied 1.0 V, there was a minor change in absorbance, but with the alternating pulses, there was no change in absorbance. It was expected that the absorbances were

proportional to the concentration of 4-chlorophenol at the main peaks exhibited by it, at 230 nm and at 280 nm. Most runs using only Na_2SO_4 and 4-chlorophenol in the electrolyte solution were inconclusive, with no major changes in absorbance and no observable trend in the hourly readings. Sometimes samples in a run taken at later times had higher absorbances than the earlier samples, which is indicative of error if a degradation reaction is occurring. Figure 14 is representative of this; it shows the absorbance measurements made for a run with 2 wt% Au/BiVO_4 . The samples taken at hour 3 and hour 4 displayed higher absorbances than the others. The remaining curves do not indicate significant degradation, signifying that 2 wt% Au/BiVO_4 demonstrated low activity with only Na_2SO_4 and 4-chlorophenol.

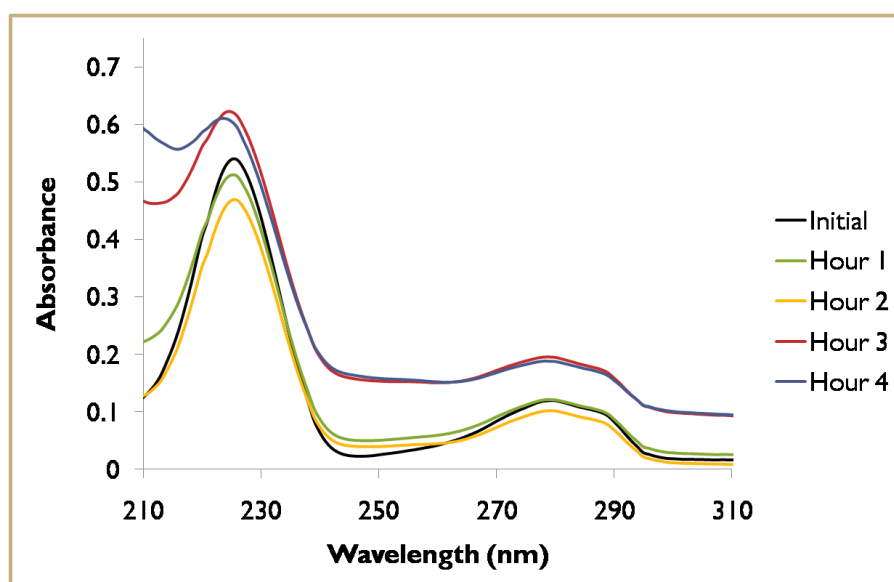


Figure 14: Absorbance of samples from 4-chlorophenol degradation with 2 wt% Au/BiVO_4 , taken once every hour. The curves were created by subtracting the blank reading from the absolute readings of the samples.

More success occurred with the addition of H_2O_2 , an electron scavenger, whereby observable changes in absorbance occurred. It was thought that the addition of H_2O_2 would promote the formation of hydroxyl radicals in the solution. As shown in Figure 15, there was a clear decrease in the absorbance readings for each hour, except that the absorbances for hour 2 and hour 3 overlapped. This may be because the vials containing these samples were accidentally mixed in the cuvette. Figure 16 also indicates that the addition of hydrogen peroxide improved the degradation efficiency. Both figures indicate that the peak at 230 nm is the one that changes the most throughout the degradation experiment; readings should be based around this peak as opposed to the one at 280 nm. The former was generated when 5 mM H_2O_2 was used, while the latter was produced with 10 mM

H₂O₂. The initial absorbance readings for each are not the same, indicating that the experimental setup must have been slightly different or that the readings were taken under different conditions (perhaps more time had elapsed between storage of the initial samples and measuring the absorbances in the second case). However, the addition of 5 mM H₂O₂ led to a degradation efficiency of 51% after the first hour and 92% after the fourth hour, based on the ratio of the change in the absorbance at 230 nm to the initial reading. The addition of 10 mM H₂O₂ resulted in a degradation efficiency of 23% after the first hour and 70.% after the second hour, which may mean that 10 mM H₂O₂ led to less effective degradation or that the samples were degraded by H₂O₂ while in storage.

These experiments should be repeated to ensure that the results are reproducible. The current results indicate that additives such as H₂O₂ should be used to study the best gold-modified bismuth vanadate photocatalysts. Unfortunately, time did not permit reproduction or further optimization of the experiments.

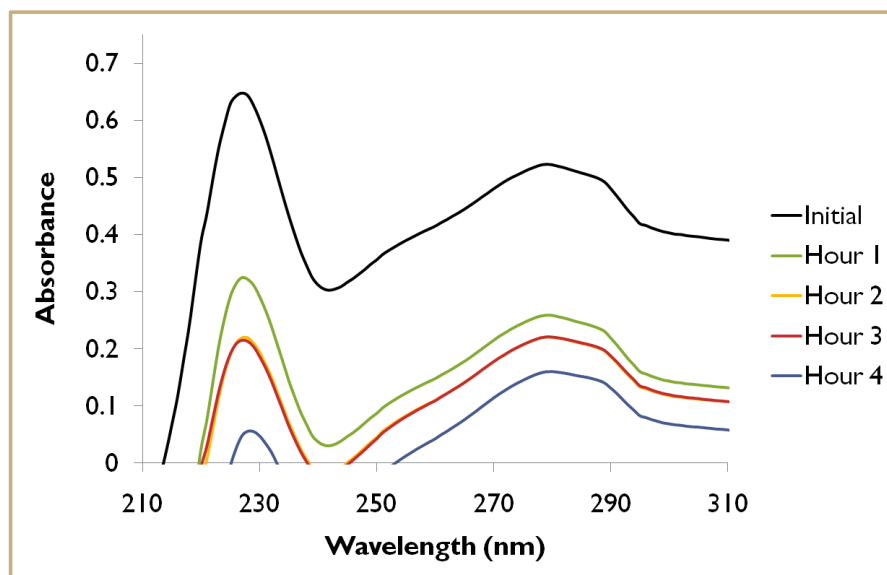


Figure 15: Absorbance of samples from 4-chlorophenol degradation with 2 wt% Au/BiVO₄ and 5 mM H₂O₂ added, taken once every hour. The curves were created by subtracting the blank reading from the absolute readings of the samples.

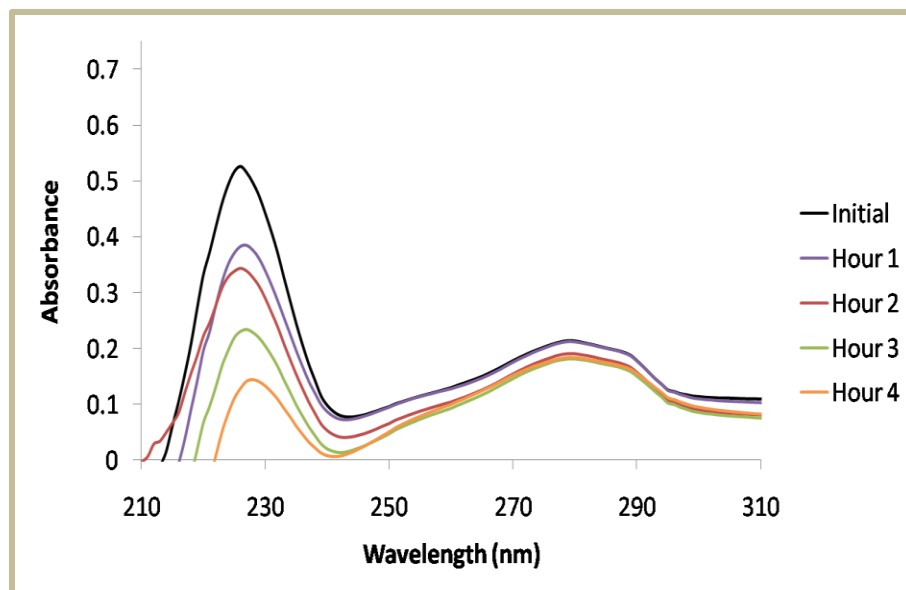


Figure 16: Absorbance of samples from 4-chlorophenol degradation with 2 wt% Au/BiVO₄ and 10 mM H₂O₂ added, taken once every hour. The curves were created by subtracting the blank reading from the absolute readings of the samples.

4.4 SEM Images

Due to limited time, scanning electron microscopy images were obtained only for the 0, 0.5, 1 and 2 wt% Au/BiVO₄ samples. The most interesting and representative images are shown in Figure 17 while the rest are in the Appendix. It can be clearly seen that BiVO₄ displays a monoclinic structure, indicating that the synthesis procedure was successful. This same structure is prominent in the gold-modified samples as well. The gold nanoparticles do not necessarily appear uniform in size but appear to be relatively “smooth” in appearance, with no spikes or right angles in their shapes. They exhibit increased dispersion at higher concentrations of gold. In the 2 wt% sample, the larger particles are on the order of 40 – 100 nm in the longest dimension. However, some small specks of particles appear to be present. It may be possible that some small clusters of gold atoms nucleated and then grew and agglomerated into the larger clusters.

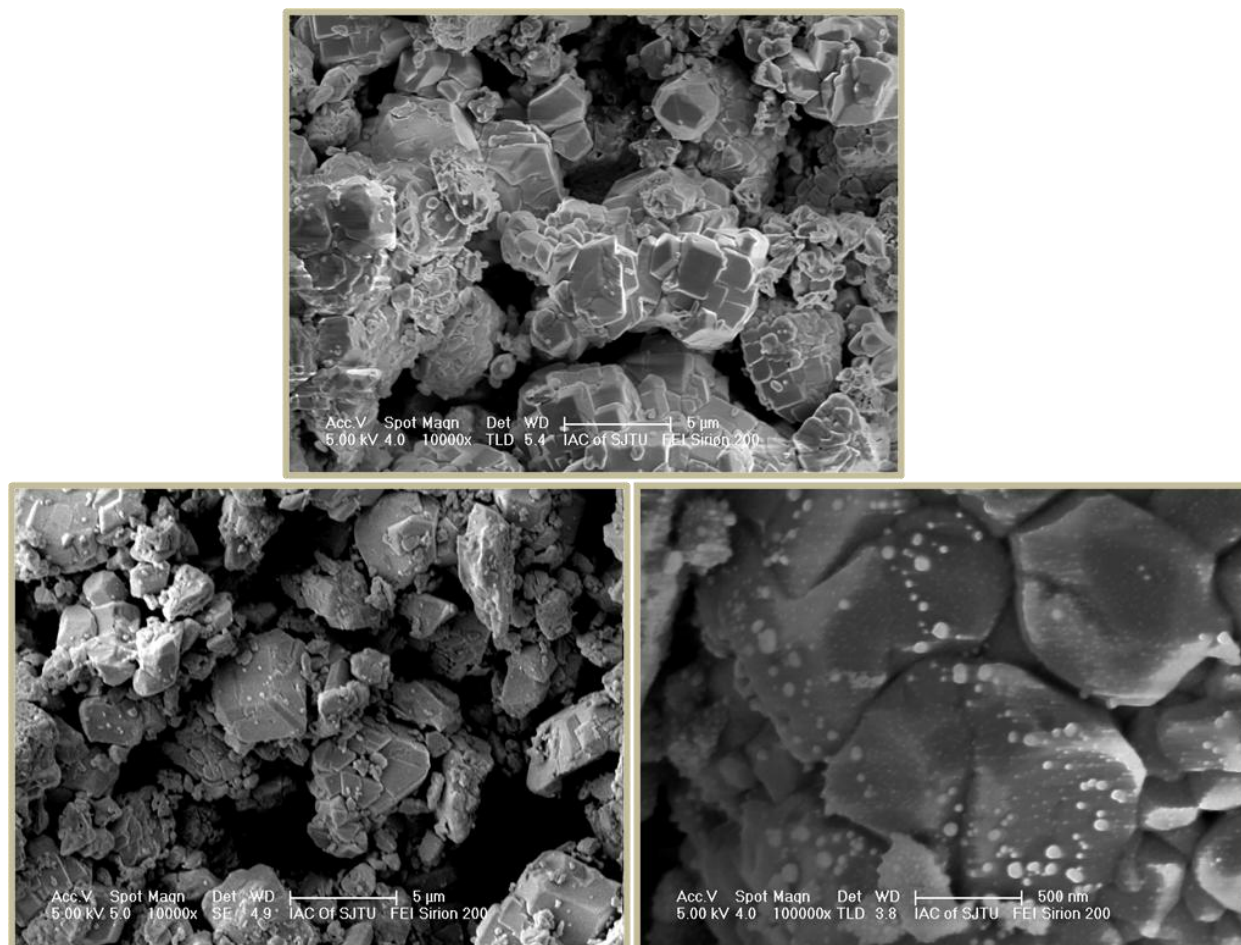


Figure 17: SEM images of (Top) BiVO_4 at $10^4\times$ magnification; (Bottom left) 1 wt% BiVO_4 at $10^4\times$ magnification; (Bottom right) 2 wt% Au/BiVO_4 at $10^5\times$ magnification

4.5 Errors and Lab Practices

Throughout the project experience, numerous sources of error were noted and are discussed in this section. These errors derive from limitations in the technology available as well as the practices employed by others in the lab.

The only available container of 4-chlorophenol was dark brown to prevent photodegradation from ambient light; however, it was broken early on in the experiment but most of the solid 4-CP was recovered and dissolved in water in a 250 mL Erlenmeyer flask. Although it was stored in a dark refrigerator, there is a possibility that this stock solution was exposed to ambient light when being used to prepare 4-CP solutions. After washing the FTO glass pieces, it was possible that they were not completely dry, dust from the air deposited on them, or that they were scratched from handling with tweezers. In the assembly of the electrochemical cell, the working electrode with the

catalyst thin film needed to be carefully placed on top of the O ring used to create a seal between it and the cell. If the electrode did slip slightly, the catalyst film could have been partially scratched off or some of the catalyst placed into the reactor cell, reducing the effective geometric area of the electrode and possibly contaminating the electrolyte solution.

Due to noise in the initial collection of data for the photocurrent experiments (without 4-chlorophenol), it was decided that the electrolyte solutions should be N₂-purged. It was necessary to redesign the reactor cell used in the degradation experiments and to change the size of the electrodes in order to create a better seal and to completely cover the O-ring. The room in which the electrochemical cell was used was relatively dark without the room lights on. To be consistent in the exposure to external light, the lights were left on in the lab. The light through the windows, which changes during the cycle of the day, was not a major source. However, the room's lights were connected to those of an adjacent lab, so others would occasionally turn off the lights when they did not realize the room was in use. The reactor cells were covered in dark paper in attempt to limit the amount light admitted by sources other than the xenon lamp. However, it was impractical to cover the removable top piece of the cell as well as the front plate of the cell and the area that it covered.

Working electrodes with visible bumps on the surface due to uneven dispersion of the paste and/or ethyl cellulose were discarded and re-made until a smooth surface was created. This does not mean that all electrodes used were relatively smooth at the microscopic level. With a smoother surface, the geometric area would more closely approximate the true catalytic surface area. The furnaces used for calcination were filled with the ambient air, so it cannot be known for certain whether undesired reactions occurred on the working electrodes at the high temperatures in the furnace or whether impurities may have been introduced.

When the degradation experiments were carried out, the absorbance data may have had serious errors in it. Although the samples were stored in a dark refrigerator and covered when transported, they may still have been exposed to light, leading to degradation not caused by the photoelectrochemical degradation. The sample port in the cell was not located immediately next to the working electrode, and the stirrer bar in the main part of the cell may not have induced mixing in the channel leading to the working electrode. This may mean that the samples taken were not truly representative of the bulk surrounding the photocatalyst. It would be recommended to thin the front side of the reactor cell, which would reduce the size of the channel between the working electrode

and the main compartment of the cell. This would also reduce the likelihood that bubbles would form and be trapped in the channel when filling the cell with solution. It is doubtful that the cuvettes used for the absorbance measurements were clean despite thorough washing from the investigator; occasionally the background curves generated with the blanks would show absorbance peaks!

In general, lab practices of colleagues were seen as poor. Oftentimes, powder residue was observed on the glassware shared with me. There was no central HVAC system in the lab building, so vapors were diluted by opening the windows in the lab or removed inefficiently by turning on a single fume hood with the sash opened above the recommended level. The floors and counters were filthy with unknown residues, and many metal cabinets (including ones for storage of chemicals) were rusted. To wash glassware, tap water, known to be biologically and chemically impure, was oftentimes used to wash the glassware, which was usually washed once before being dried in an oven where wet powder samples were dried. Many times, colored solutions were left uncovered, and labeling of containers was infrequent. In addition, there was very little urgency in the proper disposal of waste and its treatment. Powder samples and broken glassware were thrown in the regular trash, even if they contained heavy metals. There was only one waste container used for disposal of liquids and liquid-phase solutions in the labs utilized by the group. It was blue in color, with foam at the top, and reeked of the smell of heavy metals. It seemed to be leaking somewhat because when it was picked up, the cabinet floor was blue in color, with plastic from the container adhered to the floor. There seemed to be no apparent separation of wastes between acids, bases, heavy metals, and organics. Given these generally poor practices, it is unknown what effect they may have had on the experimental results presented in this report. It is recommended that future projects evaluate these issues and establish lab hygiene and safety protocols, with a member of the group or at least the building dedicated to ensuring it is followed.

4.6 Recommendations for Future Work

This work has been useful for a preliminary exploration of gold-modified bismuth vanadate as a photocatalyst for 4-chlorophenol degradation. However, numerous items can be improved and ideas covered in this work can be extended. experimental design

Some papers suggest that the chronoamperometric photocurrent will decay over very long periods of irradiation. Runs should be performed where the light is not chopped and where the chopped irradiation is carried over long periods of time, on order of thousands of seconds.^{13, 23}

The catalytic surface area should be determined.⁹ It would be useful to know the actual surface area of the catalyst so that all currents can be normalized with respect to area and compared quantitatively with other samples, as opposed to only being qualitatively comparable. The geometric area, as determined by the size of the O-ring in the electrochemical cell, is not necessarily an accurate indicator of the actual area of catalyst exposed by the semiconductor thin film. Ideally, BET or another adsorption isotherm would be done after the catalyst film is calcined on the substrate, but it could also be done on the catalyst powder prior to the paste being prepared to get the surface area per mass of the catalyst. Assuming the same mass of catalyst was used in all cases and the preparation method was consistent, comparisons between different electrode samples would be achievable.

The investigator feels that the overall experimental design was relatively poor and would recommend that the order of experiments be changed. Due to the short amount of time, the advice of the lab advisor was followed even when it may have been better to do otherwise. It would be suggested that future experiments first perform degradation experiments and systematically tune the parameters, including the weight percentage of gold. Then the LSV and CA data and SEM images should be collected in order to characterize the electrodes. Due to limited time, it was unsatisfying to be unable to compare the photodegradation efficiencies between the different electrodes, as is done in the literature.

The 2 wt% Au/BiVO₄ sample exhibited the best photoactivity and was predicted to have the most promising photodegradation efficiency, but due to a lack of time, the degradation conditions were not optimized. Future experiments should monitor the degradation concentrations over time and determine the degradation efficiency for a certain amount of time. The best results from the degradations performed in this project indicate that the first one or two hours was when the most degradation occurred. Photodegradation should be carried out with applied potential but no illumination and with illumination but no applied potential as control experiments. It would be useful to know which of the electrochemical, photochemical, or photoelectrochemical aspects have the most significant influences on the degradation efficiency. The channel in the front of the electrochemical cell should be thinned so that there is less distance between the working electrode and the main compartment of the cell. Adequate mixing may not have occurred, so the solution in the channel may have become stagnant. Due to the location of the sampling port, the sampling may not have been representative of the processes taking place at the catalyst surface. In addition, the

working electrode was located in the solution some distance apart from the other two electrodes. Although the reference electrode and counter electrode were relatively adjacent to each other in the solution, the working electrode was at a distance of at least the thickness of the front wall of the electrochemical cell (about 1-2 cm). This separation within the solution can lead to an undesirable solution resistance and a background current. Reducing this distance would then reduce the background capacitance that was observed in the chronoamperometric photocurrents.

There are many parameters that can be manipulated to optimize the degradation conditions, including the addition of electron scavengers, changing the pH, bubbling in O₂, and changing the power and spectra of illumination. As shown in this work, the addition of H₂O₂ greatly enhanced the photodegradation, as observed by the change in absorbance of the degradation samples. This work suggests that too much hydrogen peroxide may diminish the efficiency, so the initial concentration of it should be tuned. The surface plasmon resonance effect enables gold to absorb light in the UV range. To test this, the samples should be exposed to UV light separately from visible light; then the samples can be tested with both visible- and UV-light exposure. In addition, the power of the lamp and the current at which it is operating influences the intensity of light shone on the photocatalyst, which in turn affects the electron-hole generation and separation processes. This would then change rate of reaction. Most of the characterization experiments were carried out in an N₂-purged Na₂SO₄ electrolyte. Others have reported that the activity would be higher in an O₂ environment or with alternative electrolytes, such as NaOH. Oxygen should be bubbled into the solution because the degradation requires oxygen as an electron acceptor; the oxygen in the electrolyte would eventually be depleted because diffusion of air into the solution would be too slow.^{1, 11, 12} When bubbling gases into the solution, placing the experimental setup in a ventilation hood may prevent undesired trace gases from diffusing into the electrolyte. It has been reported that alkaline electrolytes lead to higher stability of and higher photocurrents for BiVO₄ film electrodes. This effect was attributed to lower accumulation of peroxide species in the solution when a photooxidation reaction was carried out.¹³ In order to explore possible mechanisms and the kinetically significant steps relevant to conditions under which environmental remediation would be performed, the products of the degradation would need to be analyzed more completely. As the parameters are modified, the mechanism may change or become more complicated. If the applied potential is too high, water photooxidation would become involved when one may want the activity to only stem from organic mineralization.

Work in the Flytzani-Stephanopolous group on gold modification of various metal oxide supports has revealed that the actual weight percentage of gold present in the sample is not a significant factor.^{35, 36} The nanoparticle clusters do not contribute significantly to the activity in the studied reactions. By leaching the clusters off and leaving only the most strongly adsorbed Au species (Au-O-Metal) in place on the surface, it was discovered that sites with only a single or few gold atoms were responsible for the activity of the gold catalysts supported on metal oxides. Thus, the shape of the catalyst is critical. More work should be carried out to study the structure effects. Although these metal-oxide supported gold catalysts were studied in steam reforming and water-gas shift reactions, it is possible that other oxidation reactions would experience such structure sensitivity.

Thus, the photocurrent activity displayed by the Au/BiVO₄ photocatalysts when different filters are applied may be explained by the fact that only gold should be responsible for the activity above the 535 nm filter wavelength (BiVO₄ no longer contributes). This activity remains the same for the different filters because only the gold is contributing. This photocurrent activity is similar for different weight percentages of gold because what truly matters is the formation of the few-atom clusters, not the major agglomerations of nanoparticles. This idea would suggest that the calcination process should be optimized to avoid sintering – migration of particles and agglomeration upon contact with each other due to the energy provided by the thermal excitation. The thermal treatment is important because it removes the volatile fraction and burns off the organics in the slurry paste.

Chapter 5: Conclusions

In this research, bismuth vanadate was identified as an n-type semiconductor photocatalyst that has the enticing property of being visible-light driven; it would be an alternative to the more popular ultraviolet-active titanium dioxide. Recent research indicates that transition metal modification of a photocatalyst enhances its activity, and gold is well known to catalyze many reactions. By modifying BiVO_4 with gold nanoparticles, the photocurrent generated under visible-light irradiation was much higher than that of BiVO_4 itself when the gold concentration was 1 wt% or more. The most promising gold-modified bismuth vanadate sample studied was identified as 2 wt% Au/ BiVO_4 , balancing low loading with reasonable activity. It exhibited the largest photocurrents in illuminated linear sweep voltammetry as well as chopped irradiation chronoamperometry. The gold promotes the separation of the electron-hole pairs once they are generated and the transfer of the holes to the electrolyte before the charges can recombine. SEM images revealed that gold-modified bismuth vanadate retains the same support structures as BiVO_4 , indicating that the dispersion of gold on the surface does not appear to promote rearrangement at the surface. The addition of 5 mM and 10 mM H_2O_2 to the Na_2SO_4 electrolyte greatly enhanced the decrease in the absorbance curves of 4-chlorophenol, specifically at 230 nm. This was attributed to the role of hydrogen peroxide as an electron scavenger; because surface peroxides can be detrimental to photocatalytic performance, the lower concentration of H_2O_2 led to higher photodegradation efficiency. Modification of the electrolyte may be necessary to improve the degradation efficiency.

The 2 wt% Au/ BiVO_4 sample appeared to have the most promising photodegradation efficiency, but due to a lack of time, the degradation conditions were not optimized. In future investigations, the degradation parameters should be optimized to demonstrate the best performance. The effects of electron scavengers, pH, O_2 , and power of illumination should be explored. Once these are appropriately tuned, the gold loading on the bismuth vanadate should be surveyed as a variable once again. The activity may be enhanced, enabling better distinction among the current curves for the 535 and 600 nm filters. In addition, the absorbance curves would be more widely spaced so that the concentrations over time would follow a consistent trend. Other techniques may be more appropriate for analyzing the products, and in more completely investigating the solution after degradation, a complete mechanism could be explored. If one wishes to use this thin film semiconductor photocatalyst in the commercial treatment of wastewater, one must keep in mind the parameters that could be realistically achieved in the actual process.

References

- (1) Hoffmann, M. R.; Martin, S. T.; Choi, W.; Bahnemann, D. W. Environmental applications of semiconductor photocatalysis. *Chem. Rev.* **1995**, *95*, 69-96.
- (2) Zhu, H.; Chen, X.; Zheng, Z.; Ke, X.; Jaatinen, E.; Zhao, J.; Guo, C.; Xie, T.; Wang, D. Mechanism of supported gold nanoparticles as photocatalysts under ultraviolet and visible light irradiation. *Chemical Communications* **2009**, *2009*, 7524-7526.
- (3) Bard, A. J. Photoelectrochemistry. *Science* **1980**, *207*, 139-144.
- (4) Kohtani, S.; Koshiko, M.; Kudo, A.; Tokumura, K.; Ishigaki, Y.; Toriba, A.; Hayakawa, K.; Nakagaki, R. Photodegradation of 4-alkylphenols using BiVO₄ photocatalyst under irradiation with visible light from a solar simulator. *Applied Catalysis B: Environmental* **2003**, *46*, 573-586.
- (5) Kohtani, S.; Makino, S.; Kudo, A.; Tokumura, K.; Ishigaki, Y.; Matsunaga, T.; Nikaido, O.; Hayakawa, K.; Nakagaki, R. Photocatalytic Degradation of 4-n-Nonylphenol under Irradiation from Solar Simulator: Comparison between BiVO₄ and TiO₂ Photocatalysts. *Chem. Lett.* **2002**, *31*, 660-661.
- (6) Subramanian, V.; Wolf, E.; Kamat, P. V. Semiconductor–Metal Composite Nanostructures. To What Extent Do Metal Nanoparticles Improve the Photocatalytic Activity of TiO₂ Films? *J Phys Chem B* **2001**, *105*, 11439-11446.
- (7) Long, M.; Cai, W.; Wang, Z.; Liu, G. Correlation of electronic structures and crystal structures with photocatalytic properties of undoped, N-doped and I-doped TiO₂. *Chemical Physics Letters* **2006**, *420*, 71-76.
- (8) Chandrasekharan, N.; Kamat, P. V. Improving the Photoelectrochemical Performance of Nanostructured TiO₂ Films by Adsorption of Gold Nanoparticles. *J Phys Chem B* **2000**, *104*, 10851-10857.
- (9) Wodka, D.; Bielańska, E.; Socha, R. P.; Elźbieciak-Wodka, M.; Gurgul, J.; Nowak, P.; Warszzyński, P.; Kumakiri, I. Photocatalytic Activity of Titanium Dioxide Modified by Silver Nanoparticles. *ACS Applied Materials & Interfaces* **2010**, 33-177.
- (10) Tian, Y.; Tatsuma, T. Mechanisms and applications of plasmon-induced charge separation at TiO₂ films loaded with gold nanoparticles. *J. Am. Chem. Soc.* **2005**, *127*, 7632-7637.
- (11) Vinodgopal, K.; Hotchandani, S.; Kamat, P. V. Electrochemically assisted photocatalysis: titania particulate film electrodes for photocatalytic degradation of 4-chlorophenol. *J. Phys. Chem.* **1993**, *97*, 9040-9044.

- (12) Vinodgopal, K.; Stafford, U.; Gray, K. A.; Kamat, P. V. Electrochemically assisted photocatalysis. 2. The role of oxygen and reaction intermediates in the degradation of 4-chlorophenol on immobilized TiO₂ particulate films. *J. Phys. Chem.* **1994**, *98*, 6797-6803.
- (13) Long, M.; Cai, W. Photoelectrochemical Properties of BiVO₄ Film Electrode in Alkaline Solution. *Chinese Journal of Catalysis* **2008**, *29*, 881-883.
- (14) Murray, H. E.; Wong, D. Toxicological Profile for Chlorophenols. **1999**.
- (15) Fiege, H.; Voges, H. -.; Hamamoto, T.; Umemura, S.; Iwata, T.; Miki, H.; Fujita, Y.; Buysch, H. -.; Garbe, D.; Paulus, W. In *Phenol Derivatives; Ullmann's Encyclopedia of Industrial Chemistry*; Weinheim: Wiley-VCH: 2010; .
- (16) Hofstadler, K.; Bauer, R.; Novalic, S.; Heisler, G. New Reactor Design for Photocatalytic Wastewater Treatment with TiO₂ Immobilized on Fused-Silica Glass Fibers: Photomineralization of 4-Chlorophenol. *Environ. Sci. Technol.* **1994**, *28*, 670-674.
- (17) Mills, A.; Hunte, S. L. An overview of semiconductor photocatalysis. *Journal of Photochemistry and Photobiology-Chemistry Section* **1997**, *108*, 1-36.
- (18) Theurich, J.; Lindner, M.; Bahnemann, D. W. Photocatalytic Degradation of 4-Chlorophenol in Aerated Aqueous Titanium Dioxide Suspensions: A Kinetic and Mechanistic Study. *Langmuir* **1996**, *12*, 6368-6376.
- (19) Fujishima, A.; Honda, K. Electrochemical Photolysis of Water at a Semiconductor Electrode. *Nature* **1972**, *238*, 37-38.
- (20) Kohtani, S.; Tomohiro, M.; Tokumura, K.; Nakagaki, R. Photooxidation reactions of polycyclic aromatic hydrocarbons over pure and Ag-loaded BiVO₄ photocatalysts. *Applied Catalysis B: Environmental* **2005**, *58*, 265-272.
- (21) Kudo, A.; Omori, K.; Kato, H. A Novel Aqueous Process for Preparation of Crystal Form-Controlled and Highly Crystalline BiVO₄ Powder from Layered Vanadates at Room Temperature and Its Photocatalytic and Photophysical Properties. *J. Am. Chem. Soc.* **1999**, *121*, 11459-11467.
- (22) Long, M.; Cai, W.; Cai, J.; Zhou, B.; Chai, X.; Wu, Y. Efficient photocatalytic degradation of phenol over Co₃O₄/BiVO₄ composite under visible light irradiation. *J Phys Chem B* **2006**, *110*, 20211-20216.
- (23) Long, M.; Cai, W.; Kisch, H. Visible light induced photoelectrochemical properties of n-BiVO₄ and n-BiVO₄/p-Co₃O₄. **2007**.
- (24) Martínez-de la Cruz, A.; Pérez, U. M. G. Photocatalytic properties of BiVO₄ prepared by the co-precipitation method: Degradation of rhodamine B and possible reaction mechanisms under visible irradiation. *Mater. Res. Bull.* **2010**, *45*, 135-141.

- (25) Sayama, K.; Nomura, A.; Arai, T.; Sugita, T.; Abe, R.; Yanagida, M.; Oi, T.; Iwasaki, Y.; Abe, Y.; Sugihara, H. Photoelectrochemical Decomposition of Water into H₂ and O₂ on Porous BiVO₄ Thin-Film Electrodes under Visible Light and Significant Effect of Ag Ion Treatment. *The Journal of Physical Chemistry B* **2006**, *110*, 11352-11360.
- (26) Sun, Y.; Wu, C.; Long, R.; Cui, Y.; Zhang, S.; Xie, Y. Synthetic loosely packed monoclinic BiVO₄ nanoellipsoids with novel multiresponses to visible light, trace gas and temperature. *Chem. Commun.* **2009**, 4542-4544.
- (27) Tokunaga, S.; Kato, H.; Kudo, A. Selective Preparation of Monoclinic and Tetragonal BiVO₄ with Scheelite Structure and Their Photocatalytic Properties. *Chemistry of Materials* **2001**, *13*, 4624-4628.
- (28) Walsh, A.; Yan, Y.; Huda, M. N.; Al-Jassim, M.; Wei, S. Band Edge Electronic Structure of BiVO₄: Elucidating the Role of the Bi s and V d Orbitals. *Chemistry of Materials* **2009**, *21*, 547-551.
- (29) Wood, P.; Glasser, F. P. Preparation and properties of pigmentary grade BiVO₄ precipitated from aqueous solution. *Ceram. Int.* **2004**, *30*, 875-882.
- (30) Yang, T.; Xia, D. Self-assembly of highly crystalline spherical BiVO₄ in aqueous solutions. *J. Cryst. Growth* **2009**, *311*, 4505-4509.
- (31) Yang, T.; Xia, D.; Chen, G.; Chen, Y. Influence of the surfactant and temperature on the morphology and physico-chemical properties of hydrothermally synthesized composite oxide BiVO₄. *Mater. Chem. Phys.* **2009**, *114*, 69-72.
- (32) Yu, J.; Zhang, Y.; Kudo, A. Synthesis and photocatalytic performances of BiVO₄ by ammonia co-precipitation process. *Journal of Solid State Chemistry* **2009**, *182*, 223-228.
- (33) Castillo, N. C.; Ding, L.; Heel, A.; Graule, T.; Pulgarin, C. On the photocatalytic degradation of phenol and dichloroacetate by BiVO₄: The need of a sacrificial electron acceptor. *J. Photochem. Photobiol. A.* **2010**, *216*, 221-227.
- (34) Herrmann, J. Photocatalysis fundamentals revisited to avoid several misconceptions. *Applied Catalysis B: Environmental* **2010**, *99*, 461-468.
- (35) Fu, Q.; Saltsburg, H.; Flytzani-Stephanopoulos, M. Active Nonmetallic Au and Pt Species on Ceria-Based Water-Gas Shift Catalysts. *Science* **2003**, *301*, 935-938.
- (36) Boucher, M. B.; Goergen, S.; Yi, N.; Flytzani-Stephanopoulos, M. 'Shape effects' in metal oxide supported nanoscale gold catalysts. *Phys. Chem. Chem. Phys.* **2011**, *13*, 2517-2527.

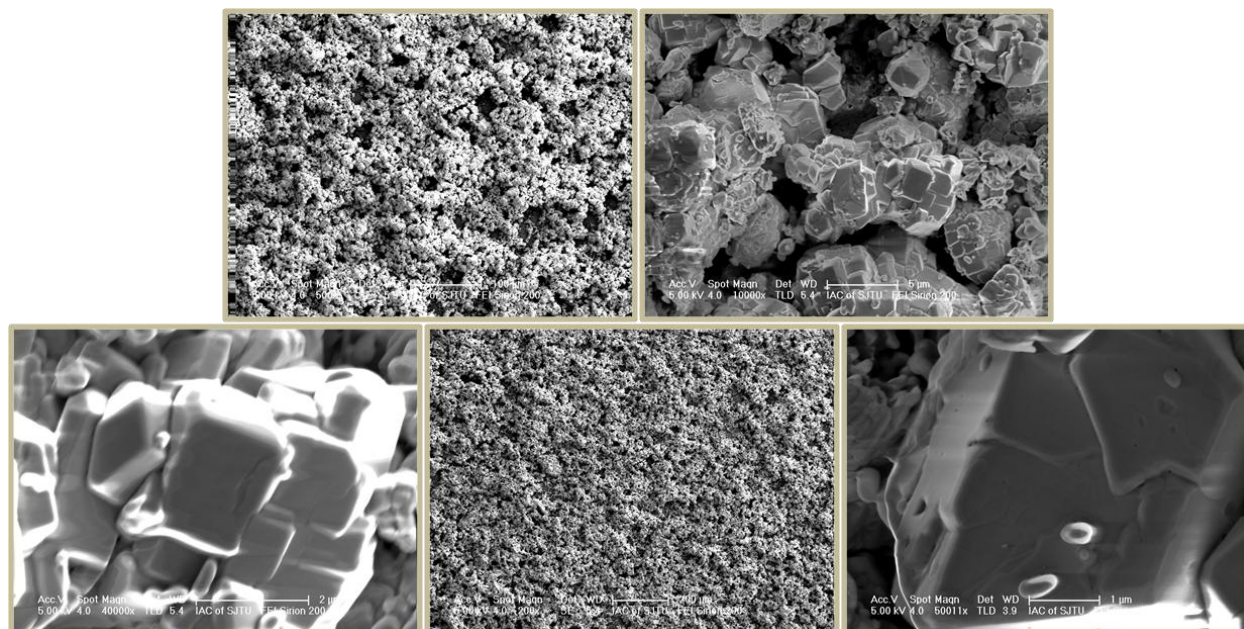
Appendix

Furnace Program for Electrode Calcination

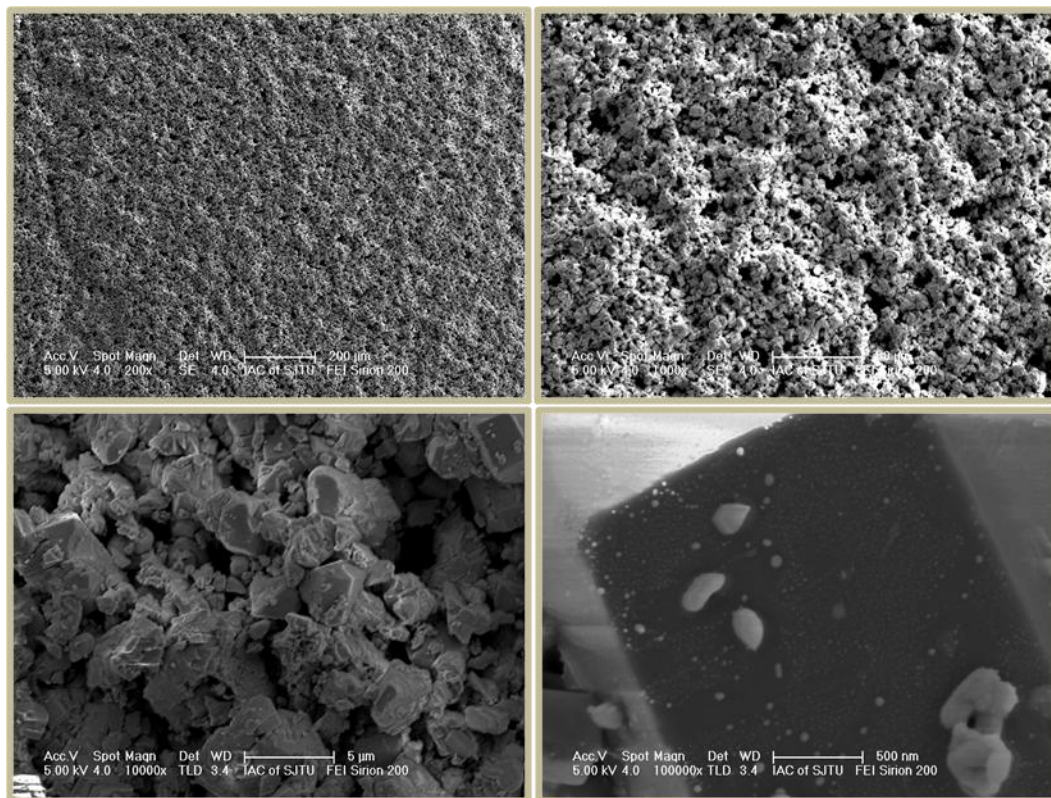
Region	Temperature (°C)	Time Interval (min)	Cumulative Time (min)
1	20	20	0
2	120	10	20
3	120	40	30
4	325	10	70
5	325	10	80
6	375	5	90
7	375	15	95
8	450	5	110
9	450	10	115
10	500	180	125
11	500	END	305

SEM Images

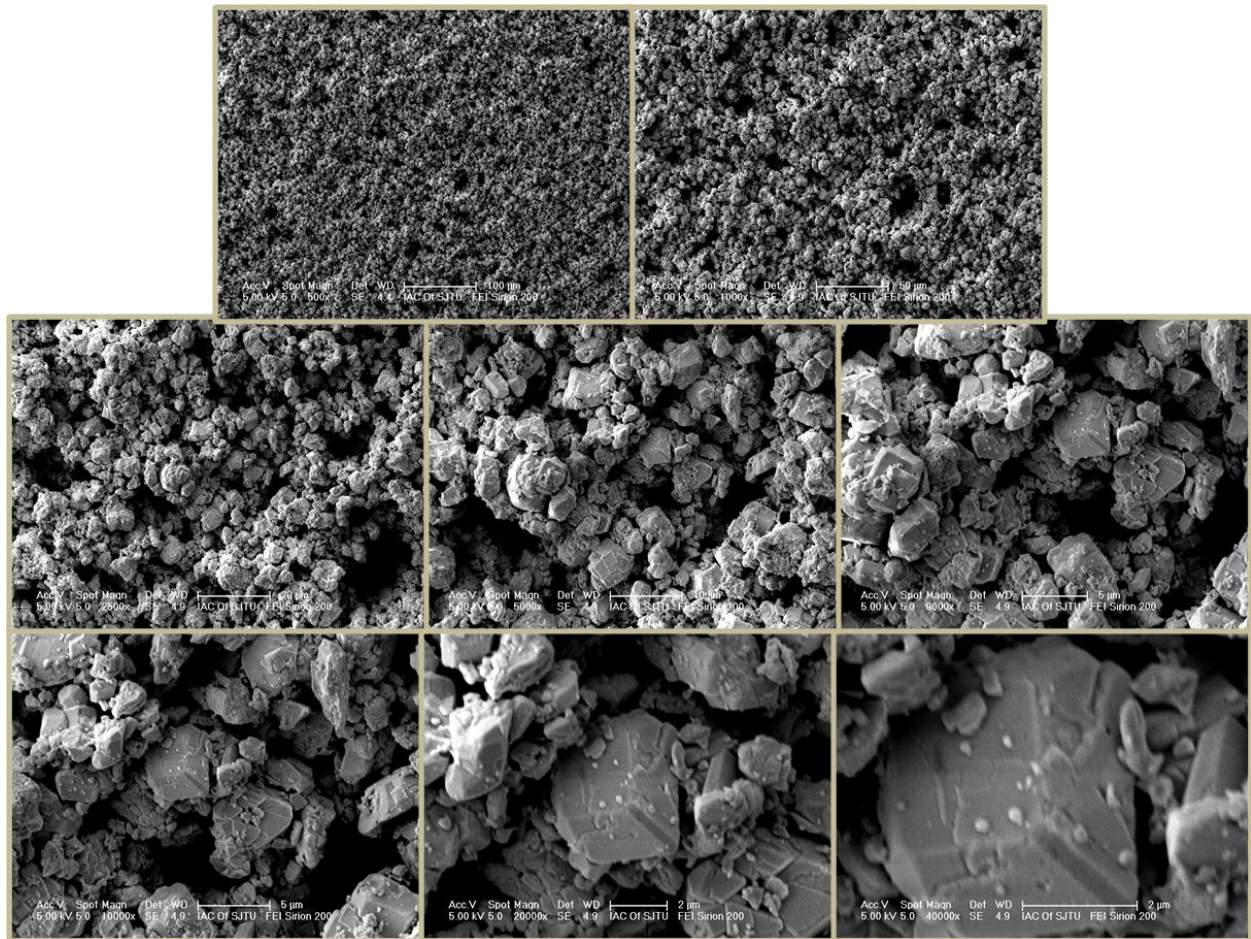
BiVO₄



0.5 wt% Au/BiVO₄



1 wt% Au/BiVO₄



2 wt% Au/BiVO₄

